UND

University of North Dakota
UND Scholarly Commons

Theses and Dissertations

Theses, Dissertations, and Senior Projects

January 2012

Vibration-Induced Atomization Of Liquids With Application To Ultrasonic Medical Nebulizers

Jesi Ehrhorn

Follow this and additional works at: https://commons.und.edu/theses

Recommended Citation

Ehrhorn, Jesi, "Vibration-Induced Atomization Of Liquids With Application To Ultrasonic Medical Nebulizers" (2012). *Theses and Dissertations*. 1236.
https://commons.und.edu/theses/1236

VIBRATION-INDUCED ATOMIZATION OF LIQUIDS WITH APPLICATION
TO ULTRASONIC MEDICAL NEBULIZERS

by

Jesi Ehrhorn
Bachelor of Science,
University of North Dakota, 2008

A Thesis

Submitted to the Graduate Faculty

of the

University of North Dakota

in partial fulfillment of the requirements

for the degree of

Master of Science

Grand Forks, North Dakota
May
2012

This thesis, submitted by Jesi Ehrhorn in partial fulfillment of the requirements for the Degree of Master of Science from the University of North Dakota, has been read by the Faculty Advisory Committee under whom the work has been done and is hereby approved.

_____
Dr. William Semke

_____
Dr. Marcellin Zahui

_____
Dr. George Bibel

This thesis meets the standards for appearance, conforms to the style and format requirements of the Graduate School of the University of North Dakota, and is hereby approved.

_____
Wayne Swisher
Dean of the Graduate School

_____
April 26th, 2012

ii

PERMISSION

Title   Vibration-Induced Atomization of Liquids with
               Application to Ultrasonic Medical Nebulizers

Department   Mechanical Engineering

Degree   Master of Science

    In presenting this thesis in partial fulfillment of the requirements for a graduate degree from the University of North Dakota, I agree that the library of this University shall make it freely available for inspection. I further agree that permission for extensive copying for scholarly purposes may be granted by the professor who supervised my thesis work or, in his absence, by the chairperson of the department or the dean of the Graduate School. It is understood that any copying or publication or other use of this thesis or part thereof for financial gain shall not be allowed without my written permission. It is also understood that due recognition shall be given to me and to the University of North Dakota in any scholarly use which may be made of any material in my thesis.

                              Jesi Ehrhorn
                              April 26th, 2012

TABLE OF CONTENTS

LIST OF FIGURES

LIST OF TABLES

Table   Page

ABSTRACT

Existing literature on the operation of ultrasonic vibrating mesh nebulizers does not entirely explain the principles by which these devices atomize liquid medication. Many of the studies on this topic assume a spray or extrusion mode of droplet generation, but it can be demonstrated that the high frequency vibration of these devices is sufficient to produce appropriately-sized aerosol droplets. A sufficiently small volume or "thin film" of liquid that is vibrated under correct conditions will produce a fountain of atomized liquid droplets which are appropriately sized for transport and deposition deep into the lungs, which is necessary for inhalation therapy. The formation of standing waves on the surface of this sort of thin film have an oscillating frequency that is roughly half the driving frequency and a wavelength that is equal to a function of the ultrasonic driving frequency, fluid density, and interfacial surface tension. The standing wavelength in particular is shown to be approximately three times the mean droplet diameter that makes up the resulting spray. Also, several studies have shown that cavitation is likely to be present in vibrating films of water which destabilize the capillary waves and may alter the overall droplet diameter distribution of the resulting fountain.

This study validates these phenomena by relating existing concepts of liquid atomization to the operating parameters of known atomizing systems and the Omron Micro Air vibrating mesh nebulizer, along with numerically altering these parameters to show trends in response conditions. A CFD analysis is performed which assists in model verification and reveals that some critical configuration driving amplitude and liquid depth must be fulfilled in order for droplet kinetic energy to exceed fluid resistance energy so that the atomization process can initiate.

The Omron Micro Air operates at an ultrasonic frequency of approximately 180 kHz and is able to maintain a liquid film that is the correct thickness to generate capillary waves leading to droplet ejection. The vibrating mesh component is assumed to be largely responsible for maintaining this film thickness along with acting as a sizing screen to only release droplets that are 3 μm or smaller. The exact function of the vibrating mesh is not analyzed in detail during this study, as the primary focus is to verify and identify parameters of atomization of a thin film of water under the aforementioned operating conditions.

CHAPTER I

INTRODUCTION

Purpose of this Study

The main purpose of the beginning stage of this research project is to define a condition at which atomization is likely to initiate under the operating conditions of vibrating mesh nebulizers. The parameters of this system are largely defined by, or coincide with, that of the Omron Micro Air nebulizer. The exact mechanisms by which these devices produce an atomized droplet fountain seem to be currently unknown in academia. At the time of this writing, the Micro Air nebulizer has been in production for about a decade and most of the studies done with and relating to it have been in the medical field, where the primary concerns include parameters such as output characteristics in comparison to other nebulizers and drug molecule preservation during the atomization process.

By defining the conditions at which atomization will occur, it will be possible for future studies to work towards optimizing the design of this type of nebulizer in terms of cost and efficiency. The cost of vibrating mesh nebulizers is largely influenced by the manufacturing processes needed to produce the vibrating mesh itself, so the detailed

understanding of how the device operates in relation to this particular component is necessary in order for any optimized design proposal to proceed.

This study explains a theory which proposes that a vibrating mesh nebulizer, such as the Omron Micro Air, produces an aerosol fountain of atomized particles simply by applying ultrasonic excitation to a thin film of liquid medication. Liquid drugs used for aerosol therapy are typically water-based and thus the properties of the majority of these fluids can be approximated by liquid water at room temperature.

It follows that an ultrasonic nebulizer can be designed to operate just as or more efficiently than existing vibrating mesh nebulizers and produce a mist of medication that is sufficient for respiratory drug delivery. Once it is understood that the correct operating conditions can be maintained with a component or components that are less expensive than the current perforated plate, the retail price of nebulizers of this type can be reduced to make the technology accessible to lower income levels which would lead to a higher quality of life for more people. Another benefit of doing away with the costly aperture plate would be the ability to produced measured-dose disposable cartridges which would virtually eliminate the time and effort spent cleaning the device of residual medication.

Vibrating Mesh Nebulizer Design

The Omron Micro Air and other vibrating mesh nebulizers have been shown to be exceptional in terms of drug delivery efficiency, operator comfort, and mildness of fluid shear strains on active drug compounds when compared to traditional nebulizers. Before the widespread use of vibrating mesh nebulizers, continuous aerosol drug delivery was accomplished by nebulizers which rely on high velocity air to shear particles of medication from the surface of a reservoir. This atomization method requires a large and typically noisy compressor that uses a relatively large amount of electrical power to operate. It also creates a very wide distribution of droplets that are propelled to the patient for inhalation at velocities an order of magnitude higher than with ultrasonic or vibrating mesh technology, and it should be noted that the inhalation of such a high-velocity "fog" of liquid medication is considered to be an uncomfortable experience, especially for young children. The use of baffles, sizing screens, and long tubes are often needed in order for the treatment to be effective at all. The whole process is very inefficient in terms of effective drug delivery and power consumption, along with poor patient comfort factors. Figure 1 shows the Omron Micro Air device and its internal nebulizer components.
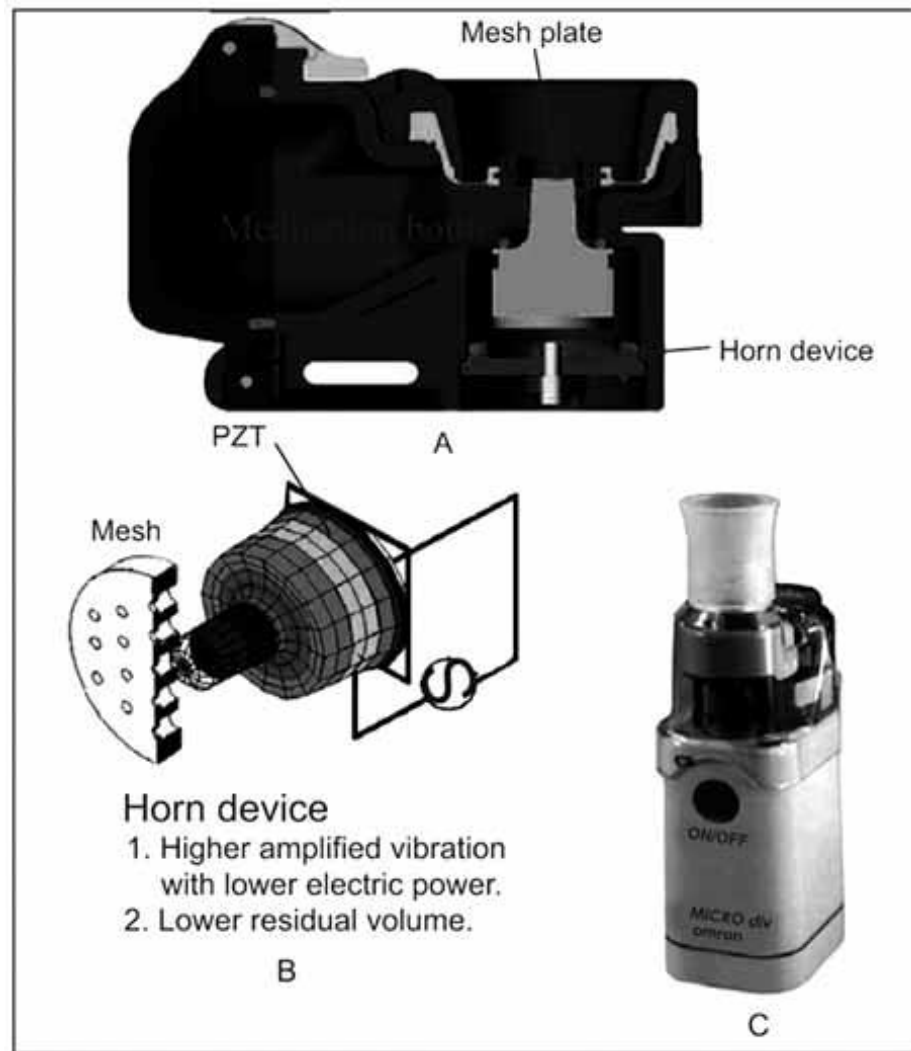
Figure 1: Omron Micro Air vibrating mesh nebulizer: Cross sections, schematic and overall design [1]

The key component of the Omron Micro Air which is under scrutiny in this study is the "vibrating mesh" itself, which is a circular plate of stainless steel that is 50 μm thick and about 5 mm in diameter. The plate is perforated with a hexagonal array of holes which are 3 μm in diameter, which corresponds to the optimum diameter of atomized droplets for effective respiratory drug delivery.

Figures 2 and 3 depict the approximate size, shape, and layout of these apertures.
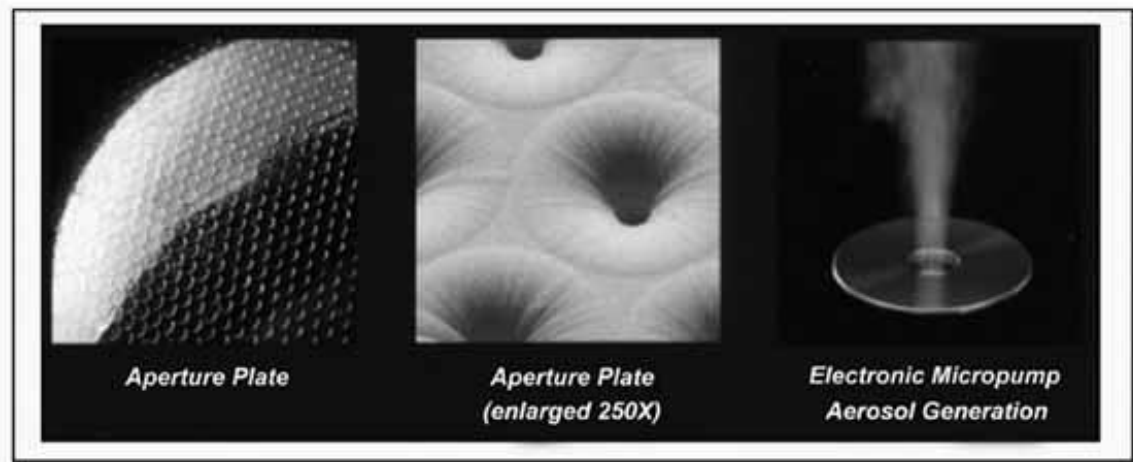
Figure 2: Omron Micro Air orifice plate: close-up orientation, geometry of outlet side, and during operation [1]
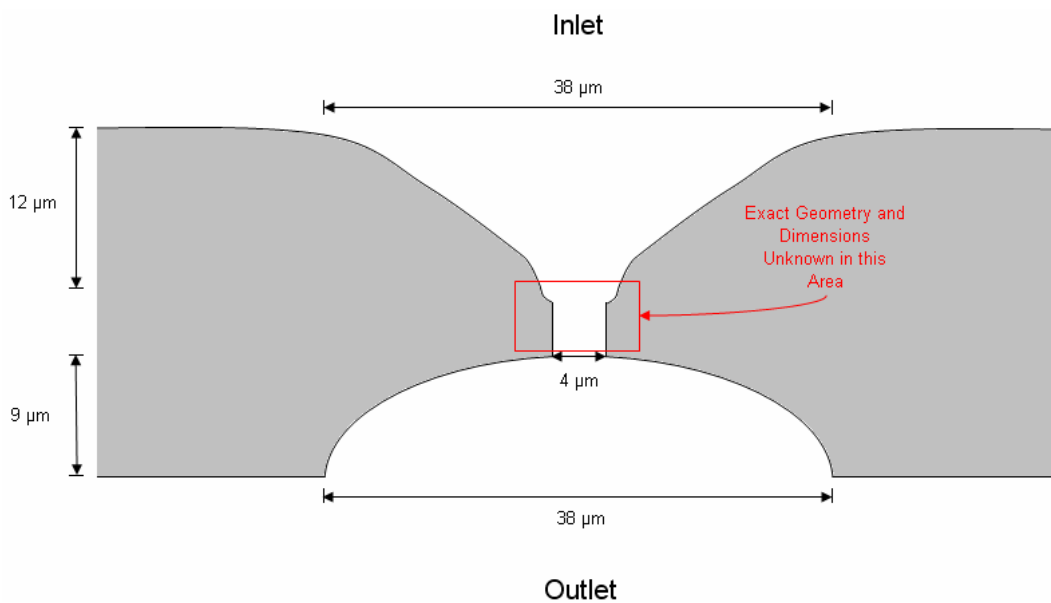
Figure 3: Approximate mesh plate orifice geometry (not to scale)

The liquid medication is held in small, clear plastic reservoir which also contains the ultrasonic actuator.   This actuator is driven by a piezoelectric transducer contained within the body of the handheld nebulizer, which also contains the control circuit, power circuit, and

power source, which for most applications and this study, consists of two AA batteries. The device is turned on and off with a single button which is set in its plastic outer shell, and since the device operates very quietly, there is a green indicator LED to display to the operator whether or not the device is working. Opposite this indicator is an orange LED which turns on once the batteries reach a low-charge state. Another small plastic piece containing the mesh plate clips onto the medication reservoir in line with the ultrasonic actuator. The mesh plate itself is supported by a relatively soft rubber ring, which allows it to move slightly while the transducer is operating beneath it.

Figure 4: Omron Micro Air operating without inhalation assist tube
Existing Theory of Operation

The mouthpiece slips over the entire medication reservoir and is ported to allow for smooth inhalation by the patient. Figure 4 shows the specific device used in this study operating with tap water.

All current literature on the performance of the Omron Micro Air and other vibrating mesh nebulizers appear to make the claim that the devices operate under a principle similar to an atomizing spray nozzle. To be more precise, this mode of operation would make it necessary for a high-velocity "filament" of liquid medication to be extruded from each orifice and undergo primary and secondary droplet breakup processes before a relatively uniform spray of droplets of appropriate size is realized. In general, this is actually a reasonable theory as it is easy to visualize and a considerable amount of work has been done in the area of atomizing spray nozzles, as well as the particle breakup phenomenon in relation to micron-order droplet sprays.

A more simplified theory often referred to as a "micropump" mode of operation, can be described as follows; a continuous body of liquid medication exists between the vibrating actuator and the orifice plate. The actuator's vibration transmits a displacement to the liquid medication, which pumps it through the orifice plate in a periodic fashion. Figure 5 depicts this process, showing that the bulk liquid body may be extruded by the vibrating mesh plate into filaments which then undergo a breakup process into atomized droplets of a desired size.
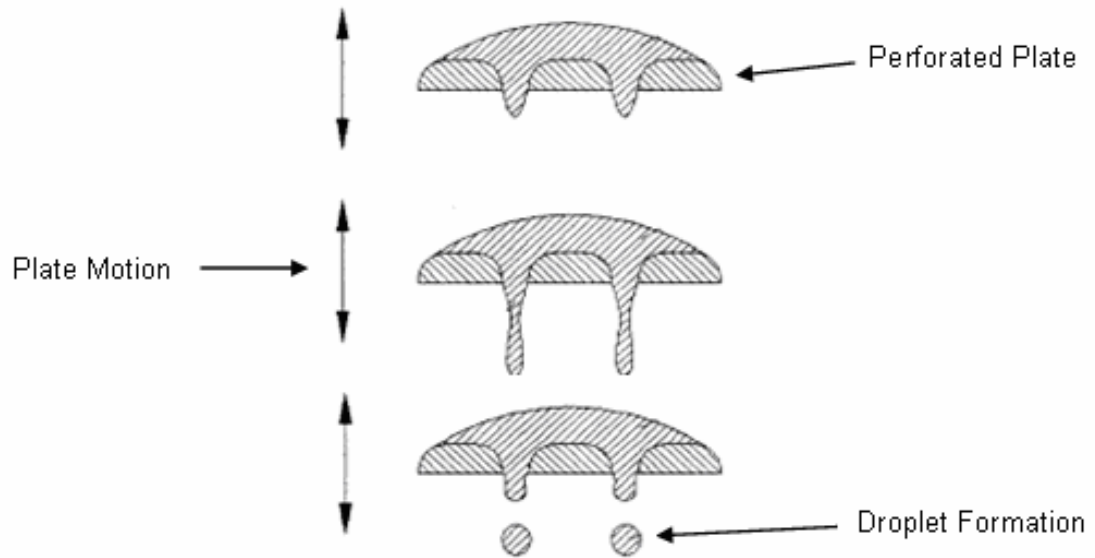
Figure 5: Vibrating Mesh Capillary Pumping Action, extrusion of droplets from bulk fluid body
(www.uspto.gov patent 5,823,428)

Either the displacement of the fluid alone or this displacement accompanied by a complimentary vibration of the orifice plate is sufficient to generate the desired droplets as the medication is passed through the holes. The exact method of how these droplets are formed in the Omron Micro Air has not been studied at length, and this is the main purpose of the study at hand. The primary problem with any kind of spraying mode of operation is the high bulk velocities involved with forming "filaments" of such a low viscosity liquid such as water. Neither the actuator nor the micro nozzles have been proven to contribute to the generation of these high velocities, which would on the order of 20 meters per second for the Omron device.

A few works of literature detailing the "micropump" theory include "A novel micropump droplet generator for aerosol drug

delivery: Design simulations" by Su, Longest, and Pidaparti [2]; "Micro-Droplets Atomizer Using PZT Ring Actuator" by Y.L. Huang [3]; "A new cymbal-shaped high power microactuator for nebulizer application" by S.C. Shen [4]; and "Influence of the vibrating system of a multipinhole-plate ultrasonic nebulizer on its performance" by Maehara, Sadayuki, and Mori [5].

Proposed New Theory

Prior to this writing and to the best of the author's knowledge, no studies relating to the operation of vibrating mesh nebulizers have proposed a theory related to the ejection of micro-droplets via standing surface waves, commonly referred to as capillary waves. The current study demonstrates that it is quite probable that the primary contributor to the generation of micro droplets in these devices is the free surface vibration of a small volume of liquid medication contained on the surface of the actuator. Many studies have clearly shown that thin volumes, or films, of various types of liquids exhibit a very pronounced surface wave phenomenon when a periodic displacement excitation is applied. A few studies have confirmed a relationship between the driving frequency of this excitation, the properties of the working fluid, and the wavelength of the resulting capillary waves. One respected theory has survived for over four decades which relates the observed surface wavelength to the mean diameter of ejected droplets, when the conditions for atomization are met or exceeded. Nearly all of these studies have dealt with working frequencies orders

9

of magnitude below that of current vibrating mesh nebulizers, but it has been stated and some evidence has been provided that the mechanics involved will "scale up" to higher frequencies. Recent work on MHz-order excitation has shown that these theories begin to break down at this magnitude, but that is beyond the scope of this study.

Within the primary focus of this study, which is to elucidate a physical mechanism for micro droplet formation in vibrating mesh nebulizers, is a proposal of the necessary conditions by which atomization will occur. These conditions are related to the constraints of known atomizers including the Omron Micro Air. It is shown that a balance between the kinetic energy of a single droplet and the surface tension energy along with a viscous resistance can be met or exceeded in order to produce conditions sufficient for droplet ejection. Another phenomenon believed to contribute to the ejection of droplets from the tips of capillary waves is that of liquid cavitation. This mechanism is most likely to occur due to very large pressure gradients formed within the vibrating film, usually near the actuator surface. The methods for testing these hypotheses include analytical calculation based on equations from existing literature and computational fluid dynamics.

CHAPTER II

LITERATURE REVIEW

Medical Background

A substantial amount of literature exists on the subject of
vibrating mesh nebulizers. Since the technology is relatively new to
the medical field, a large number of papers' primary topic is the
comparison of vibrating mesh devices to traditional air-jet devices.
The general consensus is that vibrating mesh nebulizers are superior
to their air-jet counterparts in nearly every way, and should be chosen
for use whenever possible.

Another important topic discussed deals with the handling of
certain drugs, particularly those comprised of long molecular chains.
The testing generally consists of running a sensitive liquid medication
through the nebulizer and measuring how much of it remains
undamaged before it reaches the stage of inhalation by the patient.
Vibrating mesh technology is shown to be much more compliant in the
handling of these drugs, although one study comes to the conclusion
that certain drugs require slightly enlarged holes in the vibrating plate
in order to survive the process effectively. An interesting concept to

note is that the device still produces micro droplets that are effectively sized for inhalation therapy even when the orifices are larger.

Rajiv Dhand, MD

A paper entitled "New Frontiers in Aerosol Delivery during Mechanical Ventilation" by Rajiv Dhand, MD [6] provides a brief outline of an accepted medical opinion regarding the emerging technology. In summary, it is stated that the devices produce very high fine-particle fraction aerosols and as such the efficiency of delivery to the respiratory tract is significantly higher than traditional jet or previous ultrasonic designs. It is also stated that the fine mist is generated with no internal baffling necessary, which is something that has always been used in previous designs. The statement concludes that the technology is desirable due its portability, ability to be powered by conventional batteries, ability to aerosolize solutions as well as suspensions, and the aspect of minimal residual volume of medication left over after administering the dose.

The author goes on to describe a new drug formulation at the time which is often referred to as liposome encapsulation. Essentially, the process involves spheroid molecular drug carriers which can range from nanometer scale up to a few microns in diameter. These molecular containers can transport hydrophilic compounds in their interior or lipophilic compounds in their outer membrane. These

structures are easily absorbed by living cells due to their resemblance to a natural cell structure. Previously, the main problem with delivering a drug with this method was the high rate of destruction of the liposome spheroid during atomization due to the high fluid shear induced by jet devices. Dismantling the basic structure of the container renders the necessary drug delivery mechanism ineffective.

Experimental data is provided in this paper, which illustrates a comparison between the Aeroneb Pro vibrating mesh nebulizer and the Micro Mist air jet nebulizer in the delivery efficiency of these liposome-based drug carriers. It is important to note that the Aeroneb Pro functions in a manner very similar to the Omron Micro Air, except with the orifice plate itself being oscillated directly instead of having a separate adjacent actuator. The Aeroneb Pro is shown to produce a mean particle size of 3.7 μm compared to the Micro Mist's 2.5 μm, however the Aeroneb generates a much more uniform distribution of particle size. Fine particle fraction of the Aeroneb is actually lower than the Micro Mist, which is 49% and 65% respectively. The most important point of this data is to show exactly how effective the vibrating mesh nebulizer is in comparison to its competitor, and it follows that the necessary operation time to deliver the dose is 1.8 minutes compared to 6 minutes with the jet nebulizer. Further, the estimated lung deposition is twice that of the Micro Mist. The reason

for the final two points being strongly in favor of the Aeroneb Pro is due to its delicate handling of the liposome structures, of which most survive the atomization process while relatively few survive in the competing device.

Elhissi, Faizi, Naji, Gill, Taylor

In a study on which the paper "Physical stability and aerosol properties of liposomes delivered using an air-jet nebulizer and a novel micropump device with large mesh apertures" by Elhissi et al. [7], published in 2006, the Aeroneb Pro vibrating mesh nebulizer was analyzed once again in relation to a common jet nebulizer. The paper describes the Aeroneb Pro as utilizing a dome-shaped mesh plate instead of the disc geometry found in the Omron Micro Air, but the mechanisms of operation are assumed to be very similar. In the study, a custom mesh is used in which the orifices are 8 μm instead of the typical 3 μm for these devices. The reason for the larger holes is so larger liposome-encapsulated drug structures can pass through without damage.

An important statement made by the researchers in this paper is that the performance of vibrating mesh nebulizers is largely influenced by fluid properties, namely viscosity and surface tension. It is thought that the larger liposome structures have a significant influence on the relevant properties of the carrier liquid. It follows that the drug

formulation was altered for testing purposes by way of a pre-extrusion process through a sizing filter. Unextruded, 1 μm extrusion, and 0.4 μm extrusion were compared in both devices. The dependant variable in this case is the percentage of liposome structures left undamaged through the nebulization process.
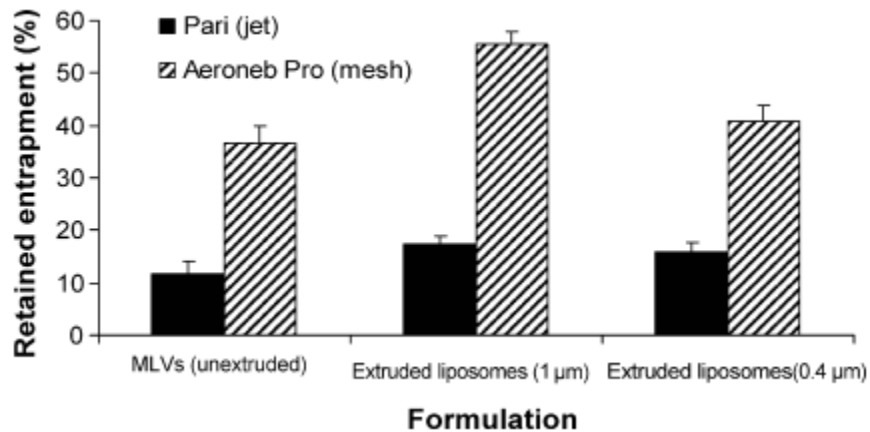
Figure 6: Retained liposomes, comparison between nebulizer types
[7]

It is easily seen in Figure 6 that of the three tested formulations, the 1 μm extrusion results in the most retained drug encapsulation. However, it is only statistically significant in the Aeroneb Pro. These data show that a significant output peak can be found at some specific fluid property value, indicating a highly fluid-dependent atomization mechanism for given mechanical boundary constraints.

Finally, the authors report an observation that through the testing process, the vibrating mesh device is a much more efficient nebulizer than the air jet device. A given volume of liquid medication is fully atomized in less than half the time by the Aeroneb Pro, which is

well illustrated by data in Figure 7 comparing the mass output rate of aerosol produced by the devices.
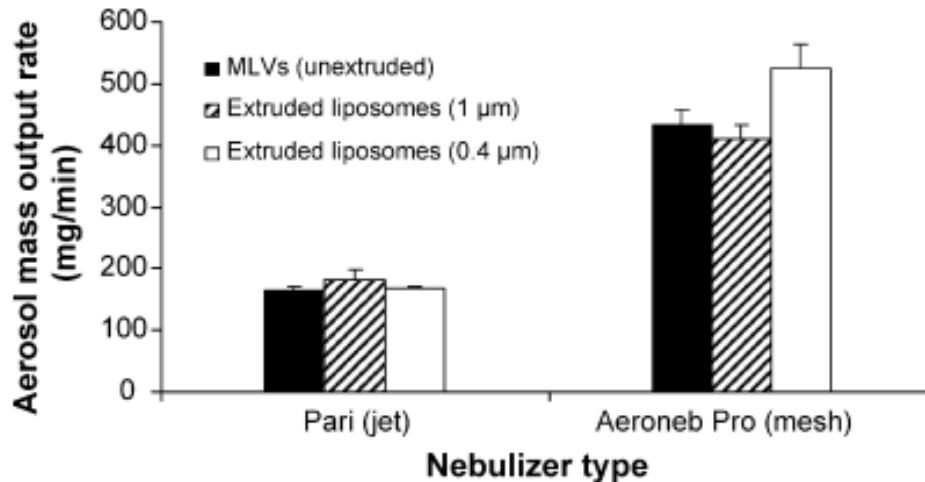
Figure 7: Aerosol output rate comparison between nebulizer types [7]

This data also shows how the output rate, much like the preserved liposome structures, exhibits statistically significant changes based on drug formulation which in this case acts to alter the fluid properties.

Other Sources

Additional literature is available which describes formed particle geometries and quality of aerosol systems as they relate to the Omron Micro Air and other vibrating mesh nebulizers. An excellent example of this includes the paper "Effect of Atomization Method on the Morphology of Spray-Generated Particles" by Eslamian and Ashgriz [8], published in 2007, which is actually written from a mechanical engineering standpoint on the formation of powders for manufacturing processes. Medical-background literature is plentiful for these devices,

and a couple of excellent works describing the physical properties of vibrating mesh nebulizers include "Advanced Nebulizer Designs Employing Vibrating Mesh/Aperture Plate Technologies for Aerosol Generation" by Waldrep and Dhand [1]; and "Current Therapies and Technological Advances in Aqueous Aerosol Drug Delivery" by Watts, McConville, and R. Williams [9]; both published in 2008. More studies which describe the interaction of various drug types and these nebulizers include "Studies on Aerosol Delivery and Plasmid DNA Using a Mesh Nebulizer" by Arulmuthu, D. Williams, Balclascini, Versteeg, and Hoare [10]; and "The influence of fluid physiochemical properties on vibrating-mesh nebulization" by Ghazanfari, Elhissi, Ding, and Taylor [11]; both of which published in 2007.

Capillary Wave Theory

Early Studies

Several works of literature were produced during an era surrounding the 1950's on the potential mechanisms of vibration-induced liquid atomization. Most of these studied focused on finite vibrating liquid films of varying thickness and the ejection of droplets from the peaks of surface waves caused by reaching unstable amplitudes or some other condition sufficient for rupture. In the case of an atomizer with a relatively low flow rate, the surface waves appear to "stand" in place while oscillating. Thus, the term "standing

surface waves" is appropriate for the system. A "capillary wave" is

technically a wave that travels across a surface (i.e. ripples), but the

waves produced by ultrasonic atomizers are often referred to as

capillary waves most likely for the sake of simplicity. It is safe to

assume that the waves traverse the surface of a small volume of

liquid, potentially reflecting at boundaries and experiencing some other

forms of bulk motion, albeit at a velocity much lower than that of the

wave oscillation and is therefore negligible for most theoretical work.

In the paper "Ultrasonic Atomization of Liquids" by Robert J.

Lang [12], published in 1962, one of the first claims of droplet size

being directly proportional to capillary wavelength is made. However,

the relationship between the frequency of surface waves and their

wavelength was published a little more than a decade earlier by

Rayleigh. An equation, often referred to as Kelvin's equation for

capillary wavelength, relating the two parameters in accordance with

the working liquids properties is as follows:

$$\lambda^3 = \frac{2\pi\sigma}{\rho f^2} \qquad\qquad \text{(Eq. 1)}$$

where λ is the surface wavelength in meters, σ is the surface tension

coefficient in N/m, ρ is the liquid density in kg/m^3, and f is the surface

standing wave frequency in Hz. The equation is reduced and the

observed phenomenon of surface vibration frequency being half that of the base driving frequency is taken into account, such that:

$$\lambda = \left(\frac{8\pi\sigma}{\rho F^2}\right)^{\frac{1}{3}}$$ (Eq.2)

Using half the base excitation frequency simply implies using the first harmonic transmitted through the fluid body. It is helpful to imagine each positive-amplitude displacement of the actuator to be driving each rise of capillary wave peaks, which are alternating evenly across the surface. This implies that the actuator is at its lowest position when the free surface is between peaks of oscillation, i.e. the surface appears flat. Thus, positive surface oscillation amplitude peaks for either "set" of waves occur on every other positive actuator amplitude peak. The mathematical derivation of this phenomenon is discussed at length in the paper "The Stability of the Plane Free Surface of a Liquid in Vertical Periodic Motion" by Benjamin and Ursell [13], published in 1954; the basis of which is the experimental studies of Faraday (1831) and Lord Rayleigh (1883), among others.

Further, Lang proposes that the mean diameter of ejected droplets is approximated by the relation:

$$D = 0.34\,\lambda$$ (Eq. 3)

This proportionality constant was obtained via an experiment in which a molten liquid wax is atomized and the generated droplets rapidly

cool in air, which are then collected and measured. In its molten

state, the liquid wax is similar in fluid properties to oils used in other

atomization studies.

Another important set of data available in this paper is that

which describes the size distribution of droplets in relation to the

driving frequency, shown in Figure 8.
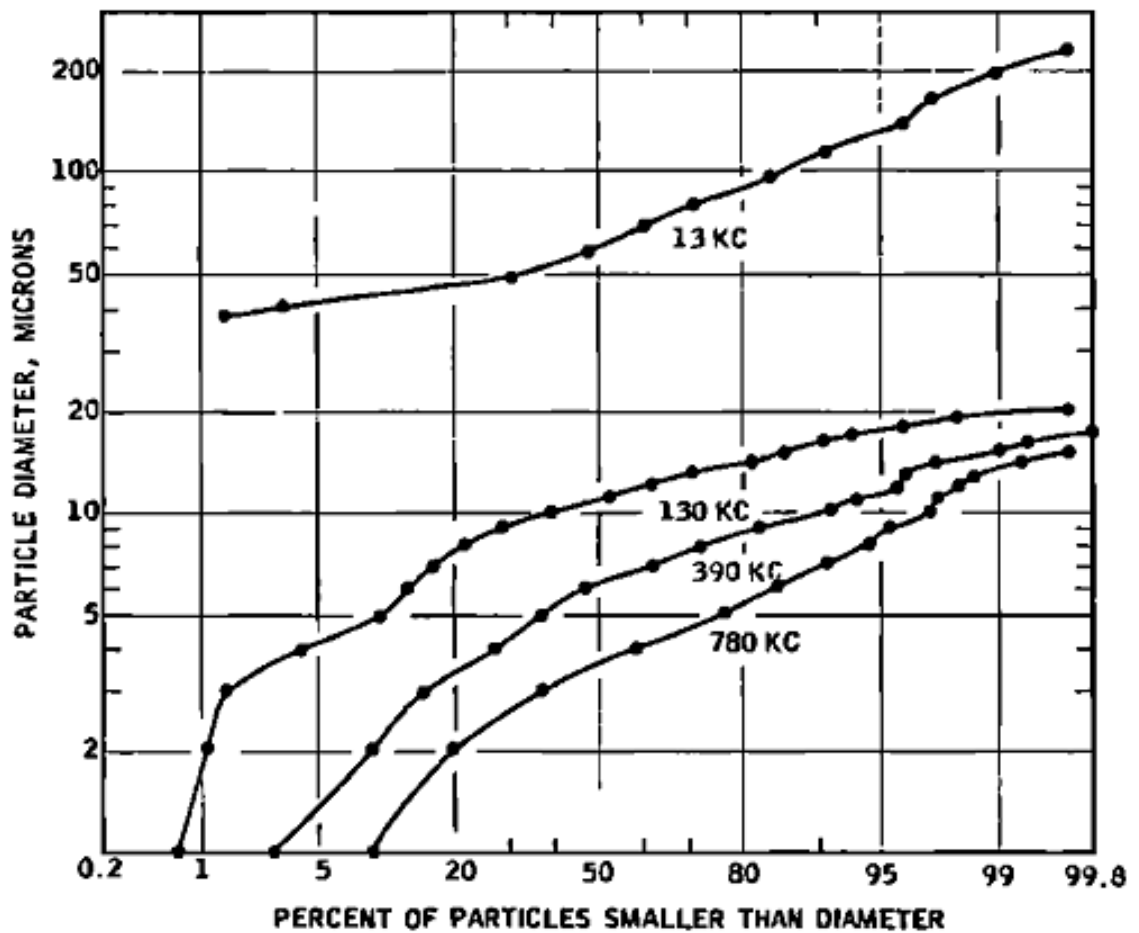
Figure 8: Particle diameter distribution comparison between
frequencies, ultrasonic atomizer with molten wax [12]

The graph shows that for the molten wax used in Lang's experiment,

the diameter of the particles ranges from as large as approximately

twice the mean down to sub-micron sizes, especially for very high

working frequencies.

Finally, Lang states that particle size tends to increase along with

atomization rate and that these results were generated at low

atomization rates. The reason for this discrepancy is most likely the

result of the conglomeration of smaller droplets into larger droplets

immediately after atomization, simply due to the inference that a

higher density fog is more likely to have its constituent droplets collide

before spreading away from one another.

An aspect of standing surface waves worth considering is if the

wave formation or shape is influenced by gravity. It is generally

accepted that at a fluid-fluid interface, surface waves shorter than a

third of a certain critical wavelength are not significantly influenced by

gravity [14]. This critical wavelength can be described as a condition

where the effects of surface tension and the acceleration of gravity are

equally responsible for the wave motion and shape. The equation for

this wavelength is as follows:

$$\lambda_m = 2\pi \sqrt{\frac{\sigma}{g(\rho - \rho')}} \qquad \text{(Eq. 4)}$$

Here, σ is the interfacial surface tension, ρ is the density of the heavier

fluid and ρ' is the density of the lighter fluid. For a water-air interface

at room temperature, the wavelength at which gravity loses significant

influence is a third of 17 mm, approximately 5.7 mm.   All systems
referenced in the current study do not generate waves this length or
longer.

Another early work of literature describing the formation of
droplets from standing surface waves from a more theoretical
standpoint is "Ultrasonic Atomization of Liquids" by Peskin and Raco
[15], published in 1963.

Contemporary Studies

Technological advancements in high-speed photography led to
further experimental study on ultrasonic atomization in the 1990's.
Photographs of initiating ejected droplets were captured in many of
these studies, but even today there are practical limitations on camera
speed when attempting to capture these effects for very high
frequency ultrasonic cases. Thus, the images available are of higher
frequency cases than what was possible mid-century and are of much
higher resolution, but the scaled-up model approach must still be
used. The most important evidence generated from contemporary
photographic study is clear sequences of still photos showing the
detachment of droplets from the tips of surface waves. [16]

The paper "Theoretical and experimental study of the behavior of
liquid film free surfaces driven by transverse ultrasonic vibrations" by
Sindayihebura and Bolle [17], published in 1995, attempts to shed some

light on the evolution of surface wave patterns during atomization. It is stated that resonance of the free surface occurs at some critical amplitude of driving surface excitation, and that the shapes of the surface vibration modes are independent of container boundary shape at any frequency high enough for producing atomized droplets. Another important point is that the early wave formation can generally be approximated linearly, while the progression of these weak surface waves to waves capable of ejecting droplets is a highly nonlinear phenomenon with the droplet ejection itself thought to be a chaotic phenomenon. Theoretical calculation in this paper shows that the excitation of unstable modes of vibration depends upon a dimensionless quantity relating the actuator acceleration to gravity, known as the Froude number. The equation is given as:

$$Fr = \frac{a_o \omega^2}{g} \qquad \text{(Eq. 5)}$$

where a_o is the driving (actuator) displacement and ω is its angular velocity. So, there is a certain critical Froude number below which the unstable modes cannot be excited. The value of the critical Froude number increases with both fluid viscosity and excitation frequency. It is once again observed that an increase in driving frequency causes the surface wavelength to decrease, further validating past studies.

The phenomenon of wave shapes or configurations as related to the container wall shape is further described in this paper. At relatively low forcing amplitudes, it is very difficult to capture a good photograph of the wave pattern but the simply observed shape is similar to that of the container (i.e. a circular container producing axisymmetric wave forms). As the driving amplitude increases, there is a chaotic transition state, then the boundary-independent square and hexagonal arrangements are observed, which tend to be much more clearly defined due to the critical amplitude being reached, and thus the excitation of surface resonance modes. The chaotic transition is most likely the superposition or interference between container dependent and independent wave shapes. After the driving amplitude is increased to show the container-independent orderly wave patterns, further increases result in the onset of atomization. A very interesting hypothesis provided for the approximately square standing wave configuration is the notion that these shapes occur due to the intersection of perpendicular plane wave modes. It follows that some form of polarization exists in the bulk body of water which guides the primary orientation of these two-dimensional waves and that any similar three-dimension system will exhibit the same phenomenon. Thus, careful consideration must be taken when analyzing the system in two dimensions. Finally, it is noted that much more complex

surface patterns are observed after atomization commences, which is

believed to be largely due to nonlinear and/or chaotic effects

originating from boundaries or other localized regions within the fluid

body, including unknown complex surface disturbances.

Further contemporary work is carried out by Yule and Al-

Suleimani in their paper "On droplet formation from capillary waves on

a vibrating surface" [16], published in 1999.
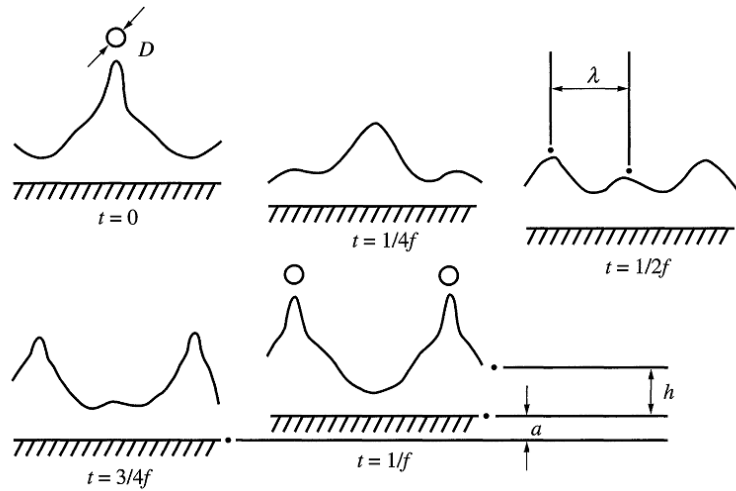
Figure 9: Illustration of droplet ejection mode during one oscillation,
ultrasonic atomizer [16]

The illustration in Figure 9 clearly depicts the authors' initial thoughts

about the appearance of one period of base excitation as related to

droplet ejection. Instead of dealing with the exact mechanisms

associated with the onset of ultrasonic atomization, observations are

made during the actual droplet ejection.

Atomization of molten solders to produce uniform spherical particulate powder is discussed. An interesting point made on this topic is that the occurrence of cavitation is improbable when atomizing a liquid metal because the vapor pressure is very low, so it should not be assumed to account for the spread in the droplet diameter distribution present in this process. Also, it is stated that the process is probably nowhere near as orderly as what is shown in the previous illustration during droplet ejection, evidenced once again by the distribution spread of droplet sizes.

Some photographs from this paper clearly show the formation of a relatively ordered wave pattern that is obscured once droplets begin to form. The authors state that every attempt so far at capturing imagery of a high-frequency, high-output fountain of atomized droplets has fallen short in the same way. The ensuing droplet cloud immediately hides the liquid surface. What follows in Figures 10, 11, and 12 is a progression of photographs showing what is described, with the first picture being the clear shot of orderly waves, then the next frame being obscured by droplets. It is clear that the ejection occurs on an extremely small time scale.
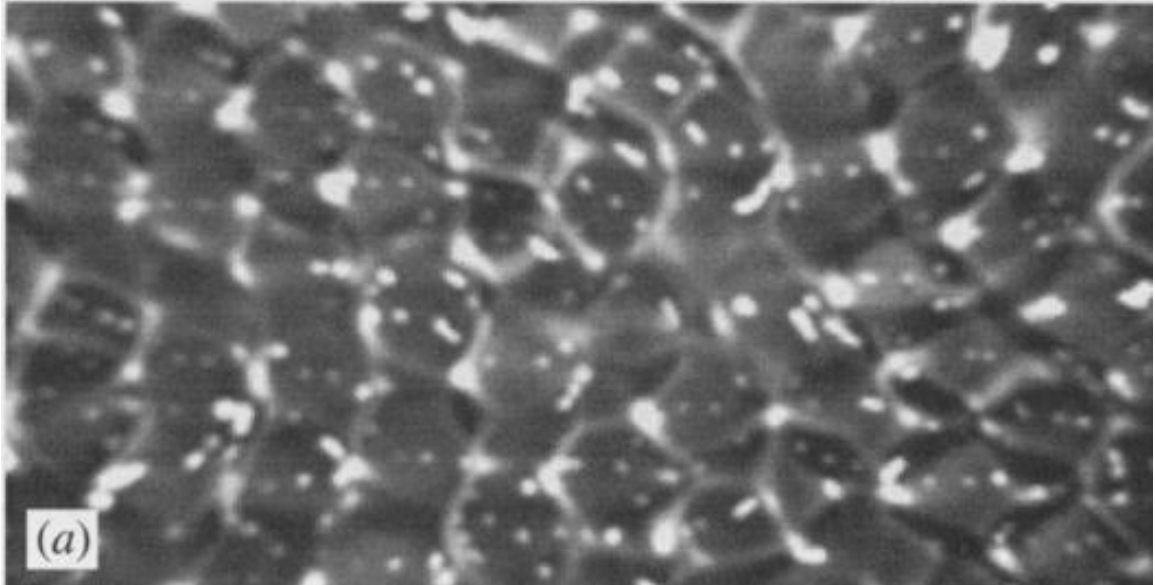
Figure 10: Wave crests inception of atomization ("choppy sea") [16]
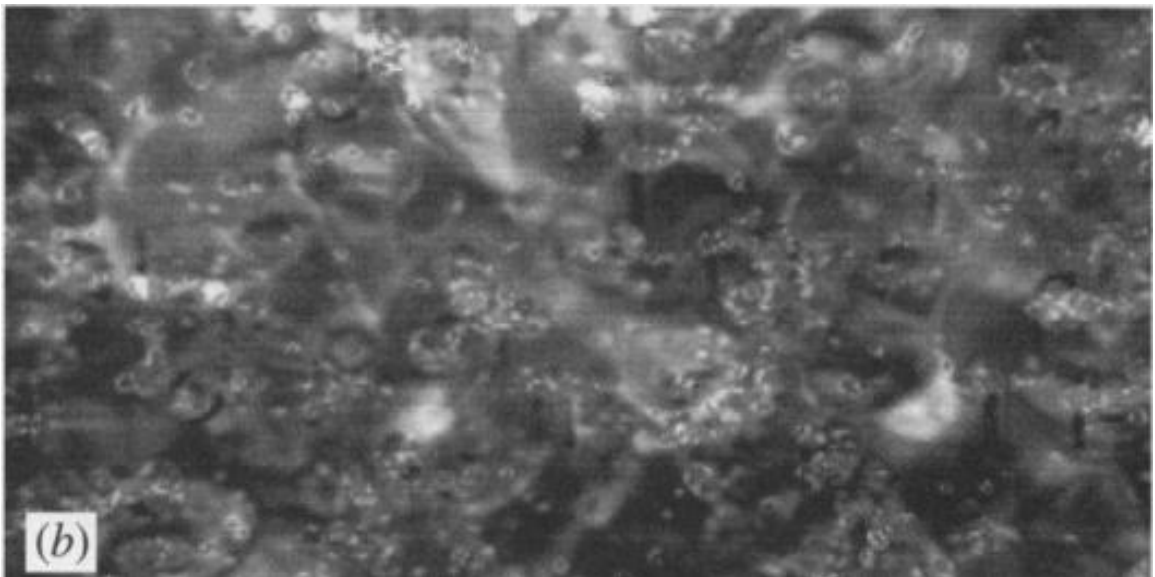
Figure 11: Atomized droplet formation obscuring previous surface
wave pattern [16]
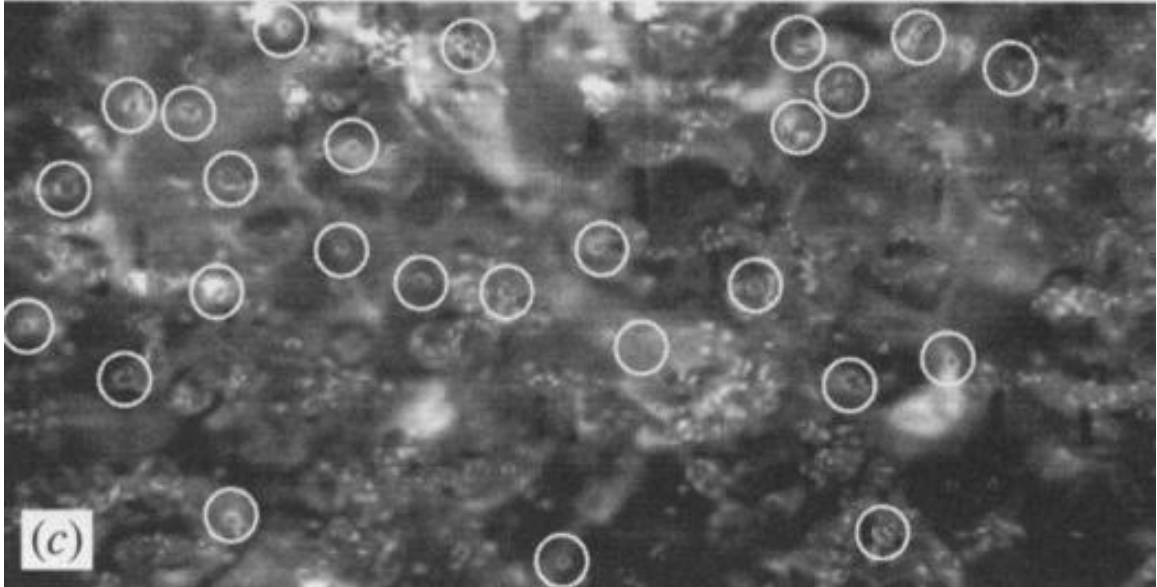
Figure 12: Individual droplets ejecting from wave crests, observed under magnified inspection [16]

The scaled-up system set up by Yule and Al-Suleimani is of great importance to the present work which will be described in detail later. Their experimental setup, shown in Figure 13 consists of a circular tray of liquid water that is approximately 40 mm in diameter. It should be noted that the exact size of the container is not nearly as important as the fluid depth (film thickness), which in this case is 2 mm. The driving amplitude is higher than the critical amplitude for capillary wave formation, and therefore the waves are independent of the container and can be analyzed in terms of expected and observed wavelengths. In this case, the driving frequency is significantly lower than an ultrasonic case at only 300 Hz but the system is scaled up to provide a more easily observed example of vibration-induced droplet formation. The driving amplitude of vibrating container is 0.1 mm.
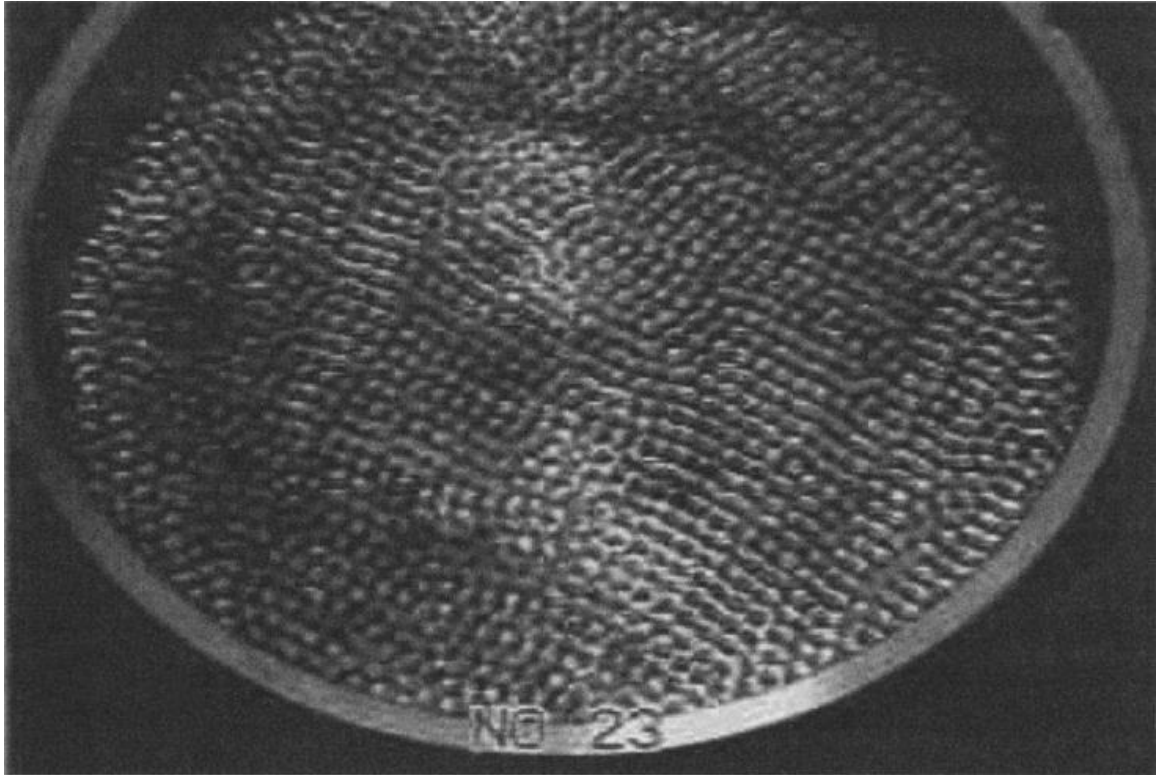
Figure 13: 300 Hz vibrating tray setup at atomization inception [16]

Another important system described by the authors is a 150 Hz setup that is run at 0.13 mm driving amplitude, which is also analyzed later in this study. Exceptional photographs were taken of this system producing droplets from capillary waves (Figure 14).
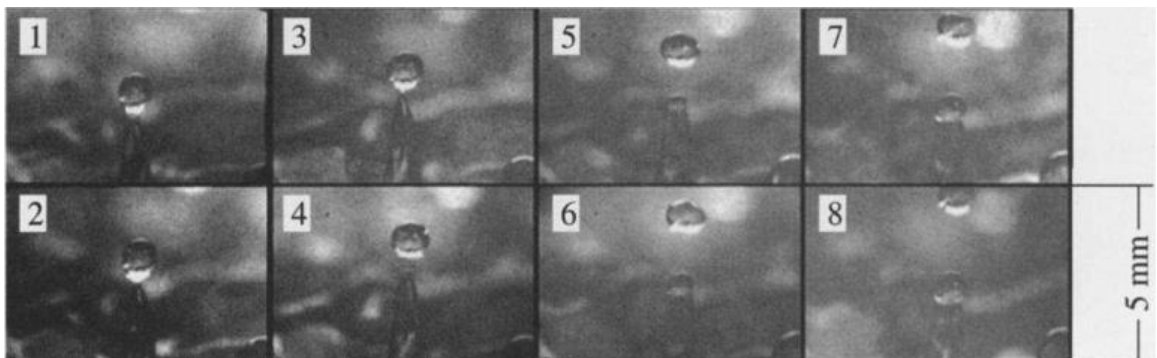
Figure 14: Frame-by-frame droplet ejection from a capillary wave tip [16]

The remainder of the paper attempts to explain why the droplet formation phenomenon is not consistent and orderly, as it is observed that a single wave cell does not continuously produce droplet after droplet. Several oscillations of the surface occur before another droplet is ejected from the unit area, during which time the cell undergoes a form of chaotic sloshing and a redistribution of liquid volume to neighboring cells. It is also observed that the lack of wave momentum which occurs prior to the next expected droplet ejection may cause a "near miss" in which a ligament stretches far enough upward but inevitably falls back downward. In this case, the following oscillation generates an excess of momentum and a very long ligament which may break up into two or three droplets of various sizes. Remembering that the droplet ejection process is expected to scale up and even at these relatively low driving frequencies the described phenomenon are occurring on the order of hundreds of times per second, it is reasonable to assume that this is a good estimate of what causes the spread of resulting droplet sizes.

In closing, it is mentioned that the film thickness reduces as the experiment is carried out because no replenishment of the operating liquid is used. However, it is stated that all photographs, observations, and measurements are taken near the beginning of atomization inception so this variation should be negligible. Very

interestingly, it is also stated that a porous wall for fluid replenishment is impractical in ultrasonic atomizer designs, but the Omron Micro Air may very well be an example of a new device which calls into question the validity of this statement.

Additional support for the calculation of capillary wavelength including a derivation which includes consideration of film thickness can be found in "Visualization and Analysis of Liquid Film Surface Patterns Formed on Ultrasonic Atomisers" by Dobre and Bolle [18], published in 1999. "Theoretical and experimental study of transducers aimed at low-frequency ultrasonic atomization of liquids" by Sindayihebura and Bolle [19] provides more background on this concept, as well as "How Orderly is Ultrasonic Atomization?" by Al-Suleimani, Yule, and Collins [20].

<div align="center">Ultrasonic Cavitation</div>

It is possible that the implosion of cavitation bubbles is a key factor in the initiation of ultrasonic atomization. This phenomenon is believed to work in conjunction with the standing surface waves, aiding in detachment through increased velocity and discontinuity but also potentially increasing the spread of the droplet size distribution in certain systems. The combined theory will be described later, but it is helpful to describe the stages and theoretical processes involved in ultrasonic cavitation prior to that. An important concept to keep in

mind is that this phenomenon is not only dependent on driving conditions but is also highly dependent on boundary conditions, the shape and size of the liquid volume, and especially the fluid properties, specifically the vapor pressure at the working temperature. The magnitude of pressure which initiates the formation and nucleation of cavitation bubbles is influenced by quasi-static pressure regions and velocity profiles resulting from pressure gradients.

"Ultrasonically Induced Cavitation in Water: A Step-by-Step Process" by G.W. Willard [21], published in 1953, elucidates a reasonable theory of the phenomenon in a very clear way. It is stated that there exists a pre-initiation condition in which a sufficiently dense field of sufficiently weak nuclei, or nucleation sites, exist in a volume of water that is being ultrasonically actuated. The true first condition is met when a weak nucleus enters a region of significantly high sonic intensity (such as a focused region or within the displacement region of an actuating surface) and grows, most likely combining with other weak nuclei. In this case, the nuclei are simply localized points of molecular attraction within the liquid volume. The weak sites become large enough to reach a resonance condition in relation to the driving frequency, which may be referred to as the second condition. Here, the nucleation site is rapidly and chaotically vibrating and changing size with the formation of a bubble being imminent in the next phase.

Once the region is sufficiently large and numerous similar sites are formed in its vicinity, the pressure gradients generated are sufficient to "tear open" a cavity of the continuous liquid, and thus a bubble is formed. It is interesting to note that a higher quantity of bubbles are generated when the water is aerated compared to when it is completely degassed, and this is likely due to existing static-pressure micro bubbles acting as nucleation sites or simply regions more conducive to nucleus growth or propagation. Finally, a post-cavitation condition also exists when the water is aerated and the large bubbles remain without collapsing.

The most important phase of this process relating to ultrasonic atomization is that where the discontinuities, or nuclei, combine and grow. It is stated that the cavitation phenomenon is much more likely to occur when standing waves are present than when traveling waves or net fluid flow is present, which are likely to cause the growing discontinuity region to "flow away" from the focal point of ultrasonic radiation. It is also very important to keep in mind that a standing wave atomization system does not necessarily need regions of the liquid body to drop below the vapor pressure. Due to the combination and growth of cavitation nuclei, a sufficient "weak point" is formed in order for cavitation to occur where it normally would not in a completely homogenous fluid body. The vapor pressure must be

achieved in flowing systems because there is no growth of discontinuities before flowing away from a region where cavitation is probable.

Other experimental work describing the presence and conditions of cavitation bubbles in ultrasonic atomization systems can be found detailed in "Ultrasonic Atomization of Liquids" by John N. Antonevich [22], published in 1957. A key experimental observation which backs up the weak-region nuclei hypothesis of ultrasonic cavitation is described in "Revealing the physiochemical mechanism for ultrasonic separation of alcohol-water mixtures" by Kirpalani and Toll [23], published in 2002.   Further description can be found in an early paper by O.K. Eknadiosyants titled "Role of Cavitation in the Process of Liquid Atomization in an Ultrasonic Fountain" [24]. An excellent section on the detection of cavitation in ultrasonic atomizers is included in the paper "Ultrasonic Atomization – a photographic study of the mechanism of disintegration" by Michael N. Topp [25].

Combined Theory

In the paper "Physical Mechanism of the Acoustic Atomization of a Liquid" by Boguslavskii and Eknadiosyants [26], published in 1967, the assertion is made that cavitation plays a major role in all ultrasonic atomization systems. In short, the ultrasonic irradiation of the liquid body generates periodic cavitation shock waves which drive the

surface capillary waves and above a certain threshold, the ejection of atomized droplets. It is pointed out that that several photographic studies employing sonoluminescence techniques have confirmed the existence of cavitation bubbles existing in droplet-producing ultrasonic fountains. It follows that a reasonable assumption can be made in which the natural oscillation of a liquid film's surface is largely influenced by cavitation phenomenon in conditions of both sonic and ultrasonic atomization. Because the previously mentioned cavitation theory states that "weak points" are present in all real bodies of liquid water, and that atomizing systems allow them to combine and grow, it is quite possible that the condition required for the initiation of atomization lies in the inherent discontinuities or nonlinearities present in any real system. An important point alluded to in the paper is that atomization can be greatly reduced or even eliminated in systems which normally eject droplets by thoroughly degassing and applying high static pressure to them. These experimental factors could effectively hold the discontinuities together to prevent the growth of disorder which normally leads to droplet ejection.

Energy Balance

In "Motion of Droplets on Solid Surface Using Acoustic Radiation Pressure" by Alzuaga, Manceau, and Bastien [27], published in 2004, a very unique and important theory in the field of liquid droplet

atomization is described. The authors have devised a set of equations

for balancing an emerging droplet's kinetic energy with resistant

energy from the fluid volume surrounding it. The primary restriction of

droplet ejection in liquids such as water and water-based medications

is the surface tension energy. This energy can be expressed simply as

the surface tension coefficient multiplied by the surface area of a

droplet to be ejected, as follows:

$$E_{st} = \sigma S_g \qquad \text{(Eq. 6)}$$

The resistant energy due to viscosity is computed by first assuming

that the flow region for a single droplet is circular in cross section and

its velocity distribution is similar to a laminar flow of the same

diameter, where after some derivation results in:

$$E_{vis} = 32\pi\mu_o r_o^3 f \qquad \text{(Eq. 7)}$$

where μ_o is the dynamic viscosity coefficient of water at room

temperature, r_o is the droplet radius and f is the surface oscillation

frequency. As previously stated, the surface waves of a base-excited

liquid film will tend to vibrate at a frequency that is half that of the

base excitation frequency. The relationship between these frequencies

has been observed experimentally in numerous studies, especially for

cases involving lower audible frequencies. The droplet's kinetic energy

is simply calculated as:

$$E_v = \frac{1}{2}\rho V_g v^2 \qquad \text{(Eq. 8)}$$

The quantities of energy of a droplet on the threshold of ejecting from the surface simply balance as:

$$E_v = E_{vis} + E_{st} \qquad \text{(Eq. 9)}$$

Since water exhibits high surface tension energy in comparison to its unit viscous energy, when calculated the viscous energy can often be left out of the balance because it is generally on the order of 1% of the surface tension energy. Thus, the balance simplifies to:

$$E_v = E_{st} \qquad \text{(Eq. 10)}$$

An application study of the droplet-energy balance method for determining the onset of atomization can be found in "Enhanced water removal in a fuel cell stack by droplet atomization using structural and acoustic excitation" by Palan and Shepard [28], published in 2006.

Atomization Parameter Studies

Quite probably the most amount of work done in relation to vibrating mesh nebulizers specifically has been on the effects of altering fluid parameters or properties on atomization characteristics. "Investigation on the Correlations between Droplet and Particle Size Distribution in Ultrasonic Spray Pyrolysis" by Wang, Purwanto, Lenggoro, Okuyama, Chang, and Jang [29], published in 2008, describes these effects from a chemical engineering point of view and

provides some images [29] to back up their claims using scanning electron microscopy. Also from a chemical engineering standpoint is "Ultrasonic atomization: Effect of liquid phase properties" by Avvaru, Patil, Gogate, and Pandit [30], published in 2005, where the fluid parameters are discussed and there are some excellent connections made on the factor of an energy balance relating to cavitation bubbles.

Finally, in "Experimental Study of Thin Liquid Film Ultrasonic Atomization" by Sindayihebura, Dobre, and Bolle [31], published in 1997, the fluid parameters influencing micro droplet atomization are well documented and connected to the authors' current and future published work. In summary, it is stated that droplet size decreases with increasing working frequency, while it increases with liquid flow rate (which corresponds to the maintenance of a thicker film) and surface tension. Droplet velocity tends to show an upward trend in conjunction with increases in both working frequency and flow rate simultaneously. However, velocity decreases as surface tension increases. These factors all act as consequential support the hypothesis that the Omron Micro Air simply operates as an optimized ultrasonic atomizer with a sufficiently thin liquid medication film.

Another excellent ultrasonic atomization parameter study is described in "Parametrically Driven Surface Waves in Viscoelastic Liquids" by Satish Kumar [32], published in 1999. Perhaps the best

resource for an all-encompassing mathematical and experimental review of ultrasonic atomization can be found in "Correlations to predict droplet size in ultrasonic atomization" by Rajan and Pandit [33], published in 2000.

CHAPTER III

EXPERIMENTAL STUDY

Experimental Setup

Analysis of the Omron Micro Air vibrating mesh nebulizer began

with a characterization study of its actuator. This was performed by

measuring its oscillating frequency and velocity amplitude with a Laser

Vibrometer. The Omron unit was simply placed onto the test stand

vertically and turned on, using its standard two-AA battery power

source. The laser measurement unit was mounted above the Omron

approximately vertical and focused onto the tip of the vibrating horn to

capture the motion. Figure 15 shows the overall experimental setup.
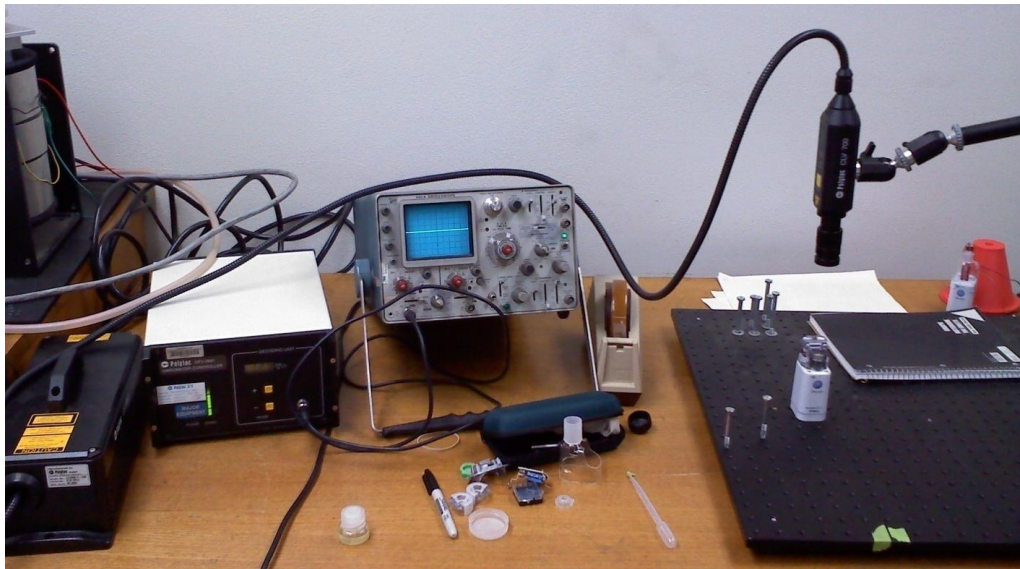
Figure 15: Overall experimental setup, measurement of Omron
actuator motion

The signal voltage was fed through an oscilloscope and the necessary

readings were made from the device's display, as shown in Figure 16.
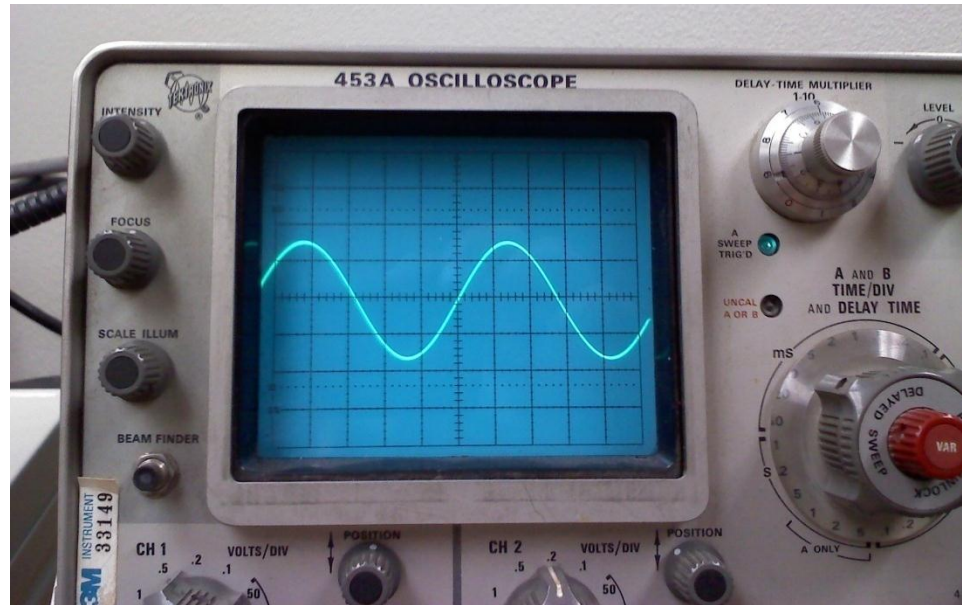
Figure 16: Clean data signal of Omron's actuator motion

A problem encountered during the initial setup phase was that

the data readout was quite noisy compared to the received signal, but

this was quickly rectified through the application of small squares of

tape to the tip of the Omron's actuator. It is believed that the

piezoelectric actuating system was simply behaving in an unstable

manner due the absence of load in the system. Once the mass of the

tape was added to the tip of the actuator, the signal noise was greatly

reduced and an accurate reading could proceed. Pictured in Figure 17

is the red laser beam focused on a black dot drawn on a small square

of green masking tape stuck to the flat actuator tip.
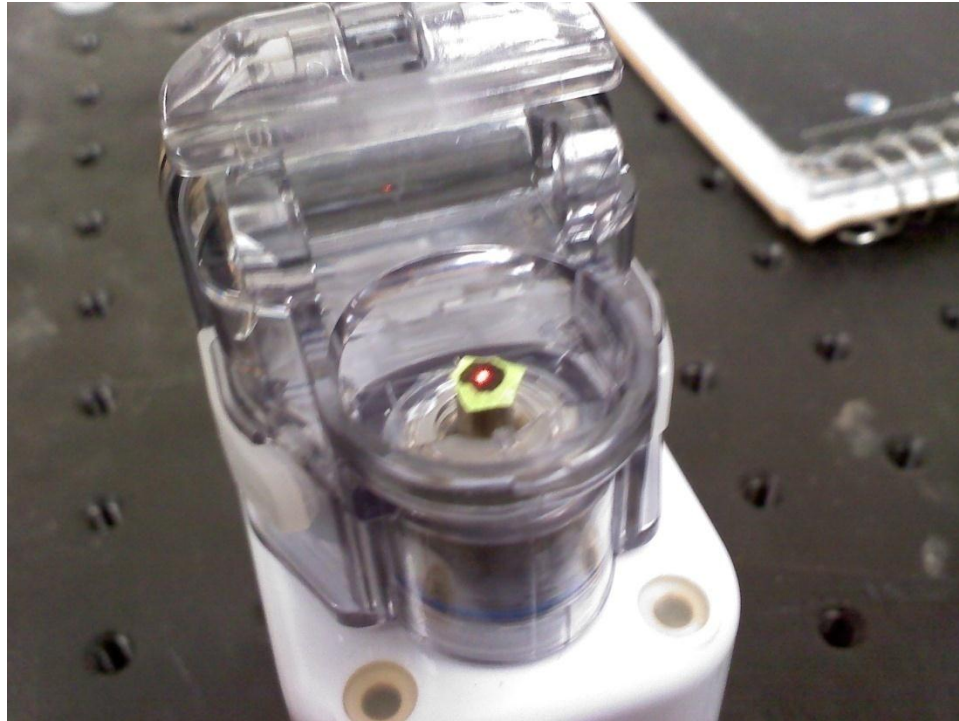
Figure 17: Tape squares applied to Omron actuator tip for clean signal

Gathering data from the vibrating mesh plate itself was also attempted but the signal could not be adequately distinguished from noise once again due to the absence of fluid load in the system. The difference between taking these readings and taking them from the actuator is that a sufficient method for applying a mass load to the aperture plate could not be found without significantly influencing its motion. The consequence of this discrepancy is that all further work done was based on the motion of the actuator alone, however it follows from the literature that the hypotheses needing to be tested for the experiment are almost entirely based on the base excitation in the system and not the flow through the mesh plate.

Measurements and Data

The actuator was found to have an oscillation period of approximately 5.6 µs based on the oscilloscope grid scale. This corresponds to an operating frequency of 178 kHz, which correlates well with the published frequency of 180 kHz. It is reasonable to make the assumption that a fairly tight spread of operating frequencies exists from unit to unit, and that the exact frequency of operation is not a determining factor on whether or not the device will operate correctly. What is probably much more important is the amplitude of the actuator, measured to peak at around 1 m/s for a minimal amount of tape applied for signal noise reduction reasons. A slightly conservative estimate of 0.9 m/s was used for the peak actuator velocity for all future calculations, which through simple integration yields a peak actuator displacement of 0.8 µm. Taking the derivative of the sinusoidal velocity equation gives peak acceleration on the order of 100,000 m/s^2, which while possible for piezoelectric crystals is not used for any practical equations of ultrasonic systems.

Observations

Only a single layer of clear plastic tape on the actuator was needed to achieve a clean signal. Beyond adding load to the system in order to get stable operation from the piezoelectric crystal, it is also possible that the tape aided in reducing unwanted reflection which

could negatively affect the laser measurement device. It is quite possible that some property of the surface finish on the actuator tip was causing the noisy readings, however simply darkening it with black ink did not help at all. It was impossible to take measurements of the actuator while under fluid load because any water on the actuator surface completely obscured the laser reflection and the resulting signal voltage.

The most important observation of the experimental research for this project was that the Omron device could produce atomized droplets without the aperture plate. Simply placing a small drop of water onto the actuator tip and turning it on resulted in an instant ejection of atomized particles. These droplets appeared to be larger than what could be produced continuously with the aperture plate in place, but this phenomenon will be discussed later. Another interesting aspect of this observation is that if a relatively large amount of water was placed on the actuator such that it appeared hemispherical, the device could be turned on and droplets would not be produced instantly. The surface of the bulk drop showed tiny ripples for a brief time, in the range of a second to a few seconds. In this configuration, the drop would eventually "break" and droplets would be ejected which ranged from on the order of a millimeter in diameter to a micron-scale fog. Even more water could be placed on

the horn tip such that the drop's surface tension was allowing it to bulge over the edge of the actuator, and in this case the droplet never ruptured and no droplets were ejected. It is also important to mention that very small amounts of water placed on the actuator would not atomize, and these bodies were generally on the order of a tenth of a millimeter in length.

Discussion of Findings

It follows that a certain amount of liquid must be maintained on the actuator tip in order to produce a constant stream of atomized droplets. The body must have enough mass and size such that a resonant mode can be excited, but not so large that the horn is not powerful enough to excite it. It should also be noted that the Omron Micro Air is touted as a low-power device, and in that way superior to traditional ultrasonic nebulizers. This study makes the assertion that the Omron device is, in fact, simply an optimized ultrasonic nebulizer. It is believed that the body of liquid medication being atomized is kept very small such that only a small amount of power is needed to get the desired effects. Traditional ultrasonic nebulizers and atomizers utilize deep pools of liquid and thus require much larger amounts of power in order to excite a resonant mode.

Even though the assertion has been made that the vibrating mesh itself is not necessary to produced atomized particles, it is still

believed to be important in the system. It may be responsible for a number of things which lead to the effectiveness of the device, but the primary theory of this study is that it maintains a certain volume of liquid, or film thickness, on the actuator tip such that a key resonant mode can be excited and that the apertures act as a sizing screen such that only 3 µm diameter droplets can escape for inhalation. In addition, it is possible that any larger droplets ejected from the film surface are extruded into a filament which undergoes a primary breakup process resulting in droplets around 3 µm.

The author of this study believes that a traditional "spray-mode" of droplet generation, like in a fuel injector, is not occurring in this system. The fluid shear resulting from the extremely high velocities necessary to force the medication through the tiny orifices would easily be on the order of or exceeding what occurs in a jet nebulizer system and it is proven that this device is much less destructive to liposome-encapsulated medications.

CHAPTER IV

ANALYTICAL STUDY

All proceeding calculation will be based on the properties of

water at room temperature (about 20-22 degrees Celsius). The

surface tension is taken to be 0.072 N/m, the viscosity 0.001 N·s, the

density 1000 kg/m^3, and all length, depth, or displacement quantities

are expressed as meters for all equations and simulations unless

otherwise noted. For the case representing the system present in the

Omron Micro Air, the actuator driving frequency is 178.6 Hz (about

1,120,000 radians per second), which is the exact calculated quantity

based on the period of oscillation previously measured to be 5.6 μs

using the oscilloscope and laser test setup.

Capillary Wave Calculations

Applying the Omron's operating frequency to Kelvin's equation

(Eq. 2) yields a capillary wavelength of 38.4 μm. Once again, this

equation does not take into account the thickness of the film and does

not account for secondary harmonics or any chaotic ripple effect of the

fluid surface brought on by droplet ejection. It also does not account

for systems in which cavitation bubbles affect the fluid surface

behavior. However, this wavelength can be thought of as an initiation

point that must be passed through in order for the Omron device to operate as expected.

Droplet Size

According to Lang's slight modification to Kelvin's capillary wavelength equation to yield an approximate mean droplet size (Eq. 3), the quantity is expected to be 13.1 μm. It should be noted that even without any of the other effects accounted for which surely reduce the mean surface wavelength, increase disorder, and cause much smaller droplets to be ejected from the surface of the film, the expected droplet size is approaching what is desired for inhalation therapy. Based on the geometry of the holes in the vibrating mesh plate, it is very reasonable to assume the possibility extrusion of this larger droplet into a filament which undergoes a breakup process into several smaller droplets. This potential phenomenon will be discussed later.

Droplet Size Distribution

It has been documented that there exists a spread of droplet sizes or diameters in all acoustic atomization processes. The mean diameter described previously is simply a value that is mostly likely to have the distribution of droplet diameters centered on it, given a certain operating frequency. In the paper "An auxiliary size distribution model for the ultrasonically produced water droplets" by

Hedrih, Babović, and Šarković [34], published in 2005, an expression is given for the probability density function of droplet diameters present in an ultrasonic atomizer.

$$f(d) = \frac{128}{3\bar{d}^4} \, d^3 \, \exp\left(-4\frac{d}{\bar{d}}\right) \qquad \text{(Eq. 11)}$$

Here, d is an arbitrary droplet diameter on the distribution curve and $\bar{d}$ is the mean droplet diameter. Once again using the mean droplet diameter previously calculated for the Omron's operating frequency and plotting Equation 9 over a range of arbitrary droplet diameters (in this case, from 1 μm to 40 μm), the following distribution is generated in Figure 18.
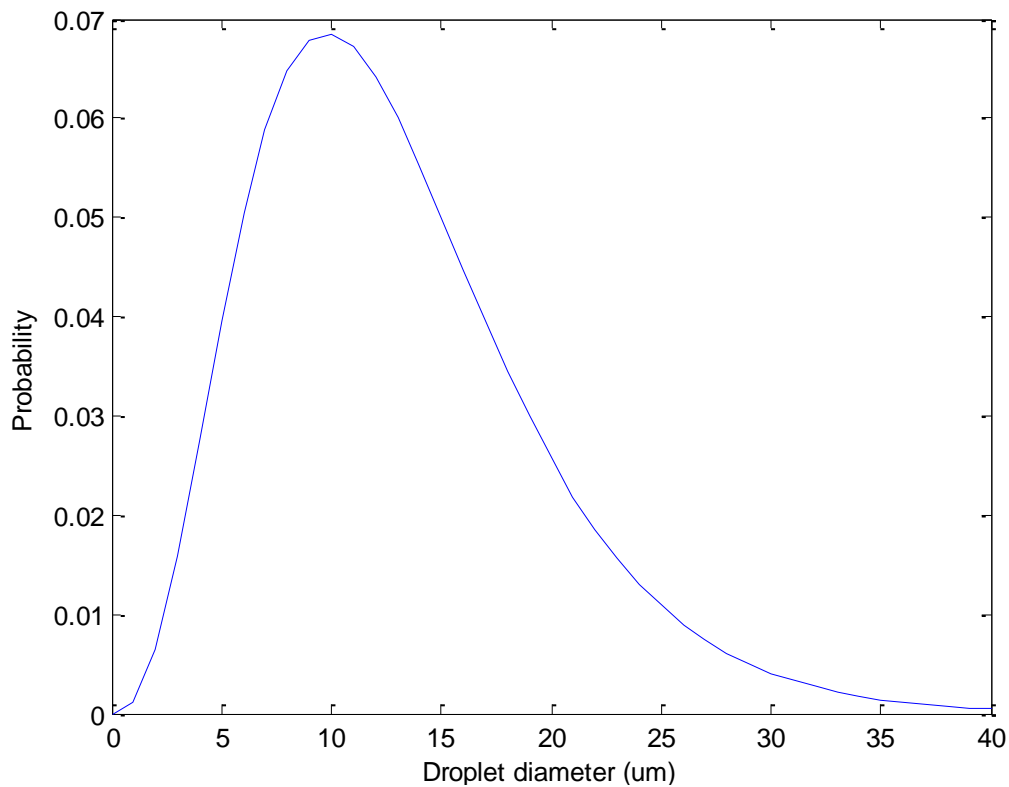
Figure 18: Droplet diameter probability density plot, Omron Micro Air operating conditions

The previously mentioned paper provides a very similar probability plot
for a 40 kHz case which has the theoretical curve along with their
experimental data points (Figure 19). This clearly shows that while
the majority of droplets are near the mean diameter, which speaks
positively about this particular benefit of ultrasonic atomizers in
general, the curve tails off toward larger droplet diameters. The data
contained in the previously mentioned study confirms that these larger
droplets exist in high frequency cases.
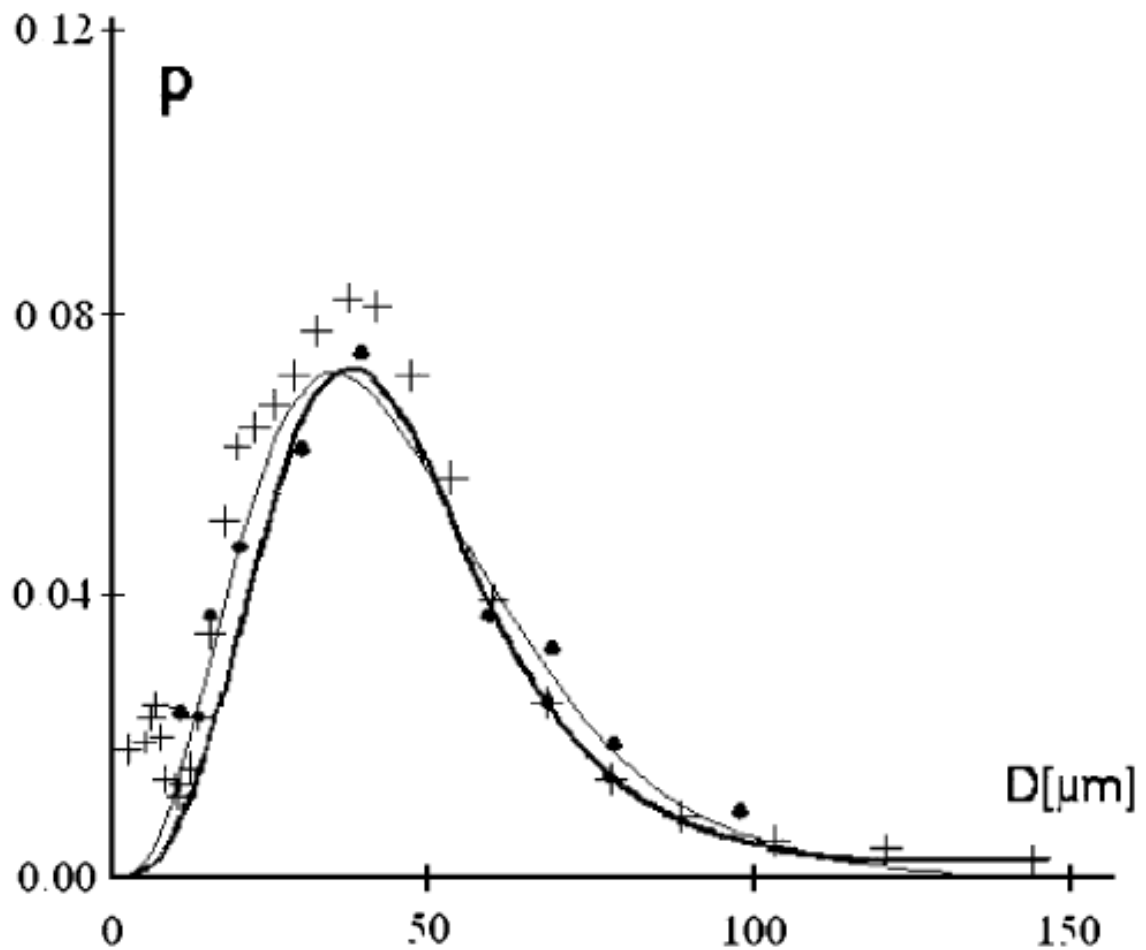
Figure 19: Droplet diameter probability plot, experimental data fit [34]

Another important point taken away from this paper is that the method for determining the droplet diameter distribution should remain valid for ultrasonic cases up to 200 kHz, meaning that the operating frequency of the Omron nebulizer is covered by this concept.

Further work describing the distribution of droplets sizes in ultrasonic atomizers can be found in "Investigation on the Correlations between Droplet and Particle Size Distribution in Ultrasonic Spray Pyrolysis" by Wang et al. [29] and in "Transient high-frequency ultrasonic water atomization" by Barreras, Amaveda, and Lozano [35]. A different approach to this concept is shown in "Application of the Maximum Entropy Formalism on Sprays Produced by Ultrasonic Atomizers" by Dumouchel, Sindayihebura, and Bolle [36].

CHAPTER V

NUMERICAL MODELING

The system that is to be used for simulation purposes is

assumed to be a representation of a wide cylindrical body of liquid

water which is vibrated normal to its free surface and is bounded by

either no-slip conditions or displacement periodicity on its outer

boundaries. The edge conditions are solver-specific and will be

discussed further in the respective constraints section for each model.

The size of the cylindrical body is calculated based on the expected

wavelength given by Kelvin's capillary wave equation (Eq. 2) which is

dependent on the base excitation frequency. According to this

equation, the wavelength expected to be produced on the surface of a

thin film vibrating on the Omron's actuator tip is approximately 38 μm.

Multiples of the wavelength quantities will be used for the size of the

CFD simulation models discussed later.

In three dimensions, the shape of the system can be visualized

as a relatively thin cylinder with its lower surface on a radial plane

which is extruded in its axial direction. Figure 20 shows an isometric

view of a solid model of the representative system.
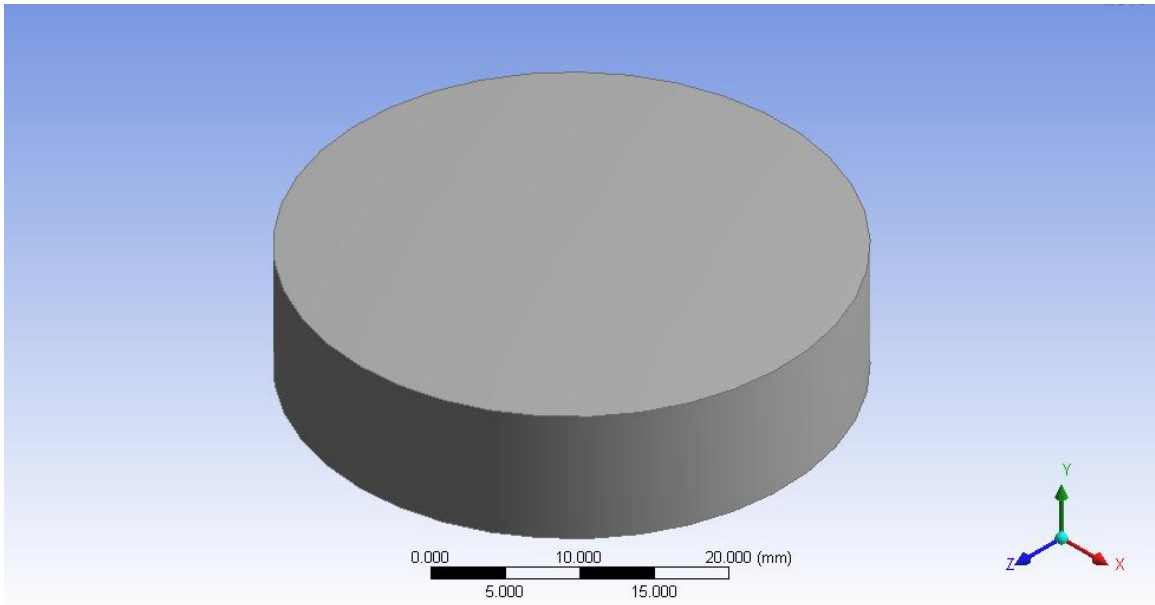
Figure 20: 3D CAD model of fluid body, isometric view
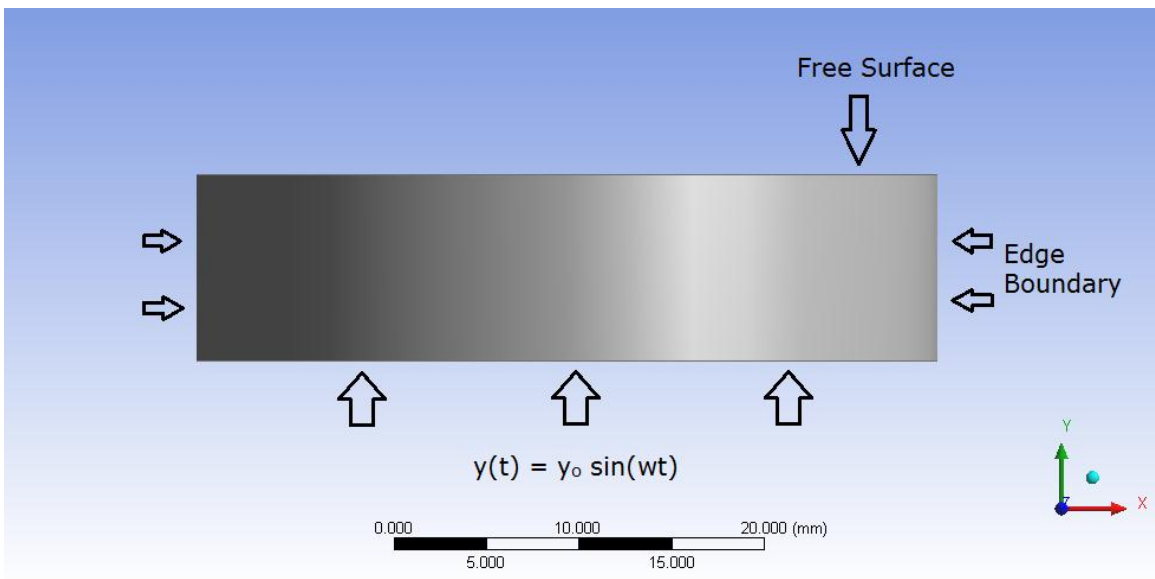
Figure 21: Overview of CFD boundary conditions, 2D plane view

Figure 21 depicts, roughly, an outline of the boundary conditions

considered. These include the displacement base excitation on the

lower circular face as a time-variable sine function, an edge condition

on the outer cylindrical face which is dependent on the choice of solver, and a free-surface condition on the upper circular face which is calculated via the Volume of Fluid (VOF) algorithm, which will be discussed later. In relation to Figure 20 and Figure 21, the acceleration of gravity is acting in the negative Y direction for the CFX model or accelerating the model in the positive Y direction for the Flotran solver (this discrepancy will be discussed further in the following model description sections).

A key parameter which is the primary distinguishing factor between the model cases is the operating frequency; the cases studied in the proceeding analyses include representations of the 150 and 300 Hz experimental setups of Yule et al. in which the excitation amplitude is clearly defined and the formation of droplets is described and confirmed, the 178.6 kHz case as defined by the operating characteristics of the Omron Micro Air device's actuator measured in the experimental portion of this study, and the loosely interpolated conditions of a fictitious ultrasonic system operating at a frequency of 70 kHz. The aforementioned low-frequency (150 and 300 Hz) cases are given the highest degree of attention due to the clearly conducted and documented study of Yule et al. in which these operating conditions were originally specified. These cases are the most reliable in terms of comparing a CFD analysis to; no other cases discovered

are as clearly defined for the parameters of interest in this study. The

178.6 kHz case representing the Omron's operating condition is

analyzed for obvious reasons and the 70 kHz case was chosen as a

rough "middle" point for verification purposes.

Flotran Model

The Flotran Computational Fluid Dynamics (CFD) solver has been

included within the ANSYS engineering analysis software package for

nearly two decades by the time of this writing. As such, its scope and

power is very limited simply due to its age. However, it is able to run

simplified systems very efficiently and has been very useful for this

study. ANSYS includes fluid elements outside of what is available for

use in Flotran, but these elements are generally only valid for

relatively low-frequency oscillations such as the case of tank sloshing

or for simply-transmitting systems such as for the acoustic analysis of

vibrating machinery. Either way, the effects of acoustic excitation on a

fluid volume or its free surface are analyses that are not valid with

these elements, which are mostly useful for fluid-structural interaction

problems.

Volume of Fluid Method

The Flotran solver includes the option to utilize the Volume of

Fluid (VOF) algorithm for analyzing fluid free surfaces. This method of

solving fluid flow problems involving free surfaces is still used today in

nearly all modern CFD solvers; notable examples include Fluent, CFX,

and Flow3D. In short, the algorithm is able to track the free surface

by including elements that are full, empty, or partially filled. The

partially filled elements are treated as polygons which are bounded by

at least one completely full element and some combination of partially

full or empty elements on the remaining sides. The calculation is

depicted geometrically in Figure 22.

(a) Original polygon (P_1, P_2, P_3, P_4) of fluid in the home element with VFRC = 0.5

(b) Advected polygon (P_1', P_2', P_3', P_4') of fluid in the next time step

(c) Intersection of the advected polygon with the neighboring elements.

(d) Update the new area and the VFRC value for the home element.
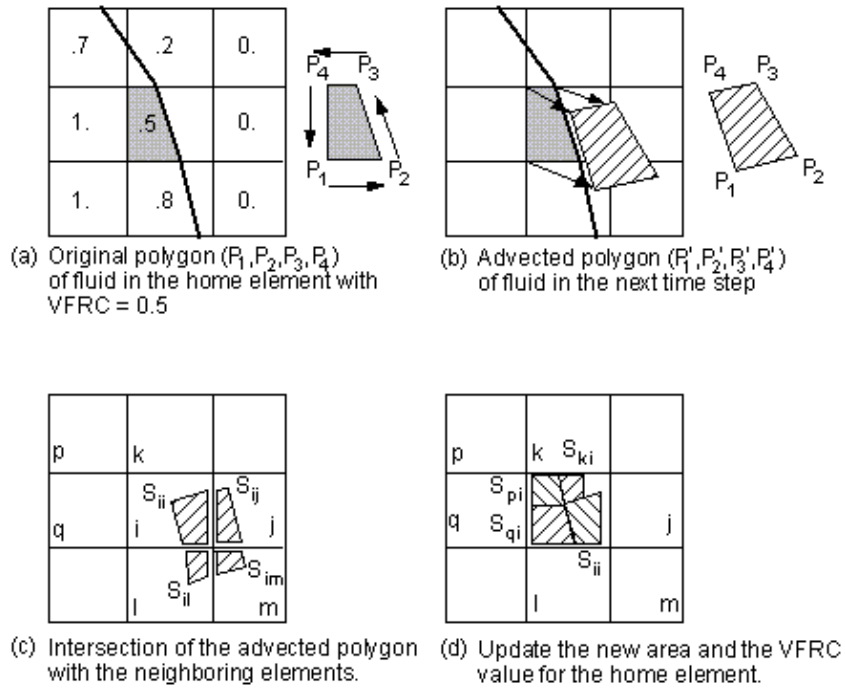
Figure 22: Geometric representation of a typical CLEAR-VOF step in Flotran CFD, ANSYS Theory Manual

The polygon is referenced as a volume fraction (denoted by

Flotran as VFRC), which is simply the ratio between the size of its filled

space and the size of a complete element. An important concept to

keep in mind is that for Flotran analyses, only the properties of the

working fluid are used for calculation. In more advanced solvers, a second fluid can be introduced as a boundary to the primary fluid. The VOF method is most commonly used for liquid water and gaseous air interactions, so any influence of the latter on the former is negligible and can simply be represented as a constant pressure for most applications. More information about this algorithm and its application in relation to the Flotran solver can be found in the ANSYS Theory Reference manual.

<div align="center">Element Overview</div>

In a Flotran analysis, the user must choose between 2D and 3D elements based on both the complexity of the model required and the limitations of the software. The primary concern of the analysis required for this study is the behavior of the free surface and because the geometry of the resulting surface waves are expected to be very small in relation to size of the bulk fluid volume, a very small portion or slice can be used effectively to yield appropriate results. Since the liquid volume is a simple film under base excitation which can be approximated as a short cylinder with a uniform surface response, it follows that a simple axisymmetric model can be used. This is of great significance because a 2D model is much easier to constrain and much less computationally demanding. In addition, the VOF option is only available for Flotran's 2D element, which is denoted as FLUID141 by

<div align="center">57</div>

ANSYS. This element provides basic flow data including velocity,

temperature, and pressure in addition to free surface tracking. The

element FLUID142 is Flotran's 3D version of FLUID141 which does not

currently support free surface analysis. More information about the

FLUID141 element can be found on the manual pages included in the

appendix.

CFD Constraints

A 2D axisymmetric model was used for all Flotran calculation.

The following image capture (Figure 23) shows an example of the

necessary mesh density and how the constraints have been placed.

The left edge is constrained such that velocity in the x-direction is

always zero at this location, which is necessary for an axisymmetric

model. The right edge is constrained in the same way, acting as a

"free slip" boundary to minimize its effects on the system. The upper

edge is constrained as a zero relative pressure boundary and the base

is set to oscillate with a displacement in the y-direction.
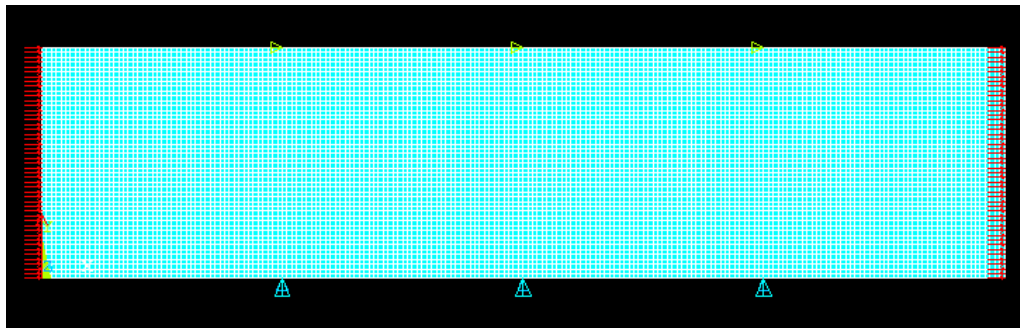
Figure 23: 2D planar Flotran model mesh and constraint indicators

This model in particular is a 300 Hz excitation case which corresponds to a system having a liquid depth of 2 mm. The expected capillary wavelength is about 2.5 mm for this low frequency system, and the model is sized at 10 theoretical wavelengths (25 mm) wide. The mesh edge length is set at 5% of the expected theoretical wavelength (125 µm) which is a consideration noted in the ANSYS documentation to be appropriate for capturing the shape of a wave (20 elements per wavelength). Verification of these parameters in particular is provided later in the Results section.
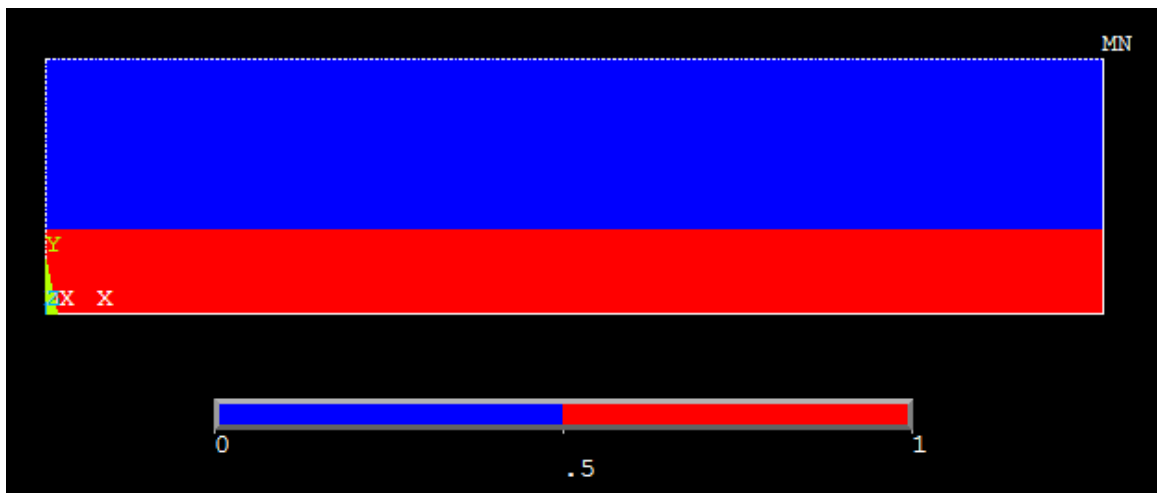
Figure 24: 2D planar Flotran model volume fraction location
(red is filled with water, blue is empty space)

In Figure 24, the lower red-colored region is the initial location of the filled liquid water elements while the upper blue-colored region is simply meshed empty space. A significant amount of empty space is necessary above the free surface so that any fluid motion that occurs during the simulation is contained within the meshed region. In a VOF

analysis, any fluid contacting an undefined or simply defined boundary

is taken to "spill into the environment" and is lost from the system. In

this case, the upper boundary is considered simply defined because it

is only a zero relative pressure condition. Applying zero velocity in the

y-direction at this edge would contain liquid but would imply a non-slip

wall, which is not an accurate portrayal of the real system.

Critical Solution Parameters

The most important observation of this study in terms of CFD

analysis is the formation of capillary waves on the surface of the

vibrating liquid film. Details on creating the model necessary for this

study could not be found at the time of this writing, so the vast

majority of the time and effort spent developing the model used for

simulation was on a trial-and-error approach of devising a numerical

method appropriate for the system. The act of developing a Flotran

model, and later a CFX model, which is able to accept the base

excitation input conditions and provide output in the form of surface

wave parameters was perhaps the greatest success of this research.

It follows that any validation property of the vibrating free-

surface model is a very important parameter to this study; details on

validation performed are included in the Results section. Critical

parameters of wave form which act as model validation include the

wavelength and oscillation frequency of the standing waves. In

addition to observing the properties of the wave formation, the peak

velocity developed in a direction normal to the actuating surface at the

tip of a given wave is also a critical parameter. This is due to the

application of this velocity magnitude in the droplet energy balance

mentioned in the previous sections. The value used for this parameter

is the peak velocity found once the surface pattern is fully developed,

or in other words, once it is not increasing in velocity magnitude any

further (steady state). Full development is easily observed and occurs

after a very short period of time, generally after only a few

milliseconds of real time for the highest frequency cases. Of course,

this may be after hundreds or thousands of time steps due to the

nature of the fluid model to develop small-scale flow which passes

through a single element very quickly. For instance, if a localized

region of fluid is flowing at a real velocity which is high enough to

cause an individual "particle" to travel farther than one element in a

single time step, the solution will diverge or will produce wildly

inaccurate results. A time step study is included later, in the Mesh

Study portion of the Model Verification section.

<div align="center">CFX Model</div>

<div align="center">*Overview of Solver*</div>

In addition to the Flotran CFD model, late in the research

process of this study a more advanced model was developed using the

<div align="center">61</div>

modern CFX solver package included in ANSYS Workbench. This

software is much more powerful than the aging Flotran code, allowing

for the specification and adjustment of many more model and solution

parameters. However, the drawback to all of this available

customization and parameter tweaking is that much more time is

needed to achieve a completely stable and accurate model. Another

negative aspect compared to the Flotran model is the length of CPU

time required of the available computer hardware to complete a single

analysis, which was generally an order of magnitude higher when

running models of the same mesh density. A large part of this

increased demand in computational resources is because CFX is strictly

a three-dimensional solver, so it must calculate the motion of fluid

hexahedron instead of a simple polygon in a VOF analysis. Also,

empty space for the liquid to flow into is not valid in this solver, so

what can be left as empty space in Flotran must to be specified as air

in CFX. However, some very interesting results were generated using

CFX which include the formation of perfectly uniform standing surface

waves, due to its advanced settings for boundary conditions which are

discussed in the next section.

Model Constraints

Similar to the Flotran model, the CFX model utilizes a sinusoidal

displacement base excitation and a zero relative pressure boundary on

the upper face. Due to advancements in usability of the solver, real-world representations can be applied to boundaries instead of simple mathematical conditions. The base excitation boundary, or actuator location, was specified as a no-slip wall for most solver runs. The pressure boundary on the upper face was able to be set as an opening, which is very commonly used in free-surface analyses. Even though the model was required to be three-dimensional, meshing a thin geometry as one element in thickness allows for the approximation of a 2D system. On the model planes normal to the thickness direction, a symmetry boundary condition was placed which specifies the geometry as a single "slice" of a larger fluid volume. Finally, the most important difference compared to the Flotran model is the use of a periodic boundary condition on the outer edge faces. This type of boundary simply translates any fluid motion from one side of the boundary to the other, which essentially eliminates any potential effects of a wall on the motion of the fluid volume. In other words, the velocity and volume fraction profile which exists at one edge of the model will simultaneously exist on the other edge. A concern of this type of boundary is excessive accumulation of flow velocity through the system due to its theoretically continuous nature, and options are available which limit this development. For the model used in this study, this was unnecessary because the fluid volume appeared to remain in place throughout the solver run.

CHAPTER VI

RESULTS

Flotran Solver

Model Verification

The first step in the process of analyzing standing surface waves

is to create a model that behaves as expected. Based on photography

and sketches from previous work, the general appearance of such a

system is known. A major problem with creating the model was that

very little assistance was available and examples of similar systems

could not be found even after an extensive search. Despite this lack of

helpful known information, through a very laborious trial-and-error

approach, a two-dimensional vibrating surface wave model was

created in ANSYS Flotran. Some rough guidelines for setting the

variables of a free surface model in Flotran were found in the ANSYS

Help documentation.

As previously stated, the first model generated which showed

surface waves forming and oscillating on the surface of a fluid body

was planar rectangular system without axisymmetry specified.

Screenshots a model similar to this first one generated can be seen

64

in Figure 25; in this case, the model is driven at 300 Hz with a base excitation amplitude of 0.1 mm, its depth (later denoted as thickness) is 2 mm, and its width (later denoted as model size) is 10 theoretical wavelengths. At 300 Hz driving frequency, a theoretical wavelength is 2.5 mm and therefore the model is 25 mm wide. The mesh edge length used is 0.125 mm and the time step is 0.1125 seconds (the reason for the use of these specific values will become clear in the proceeding sections).
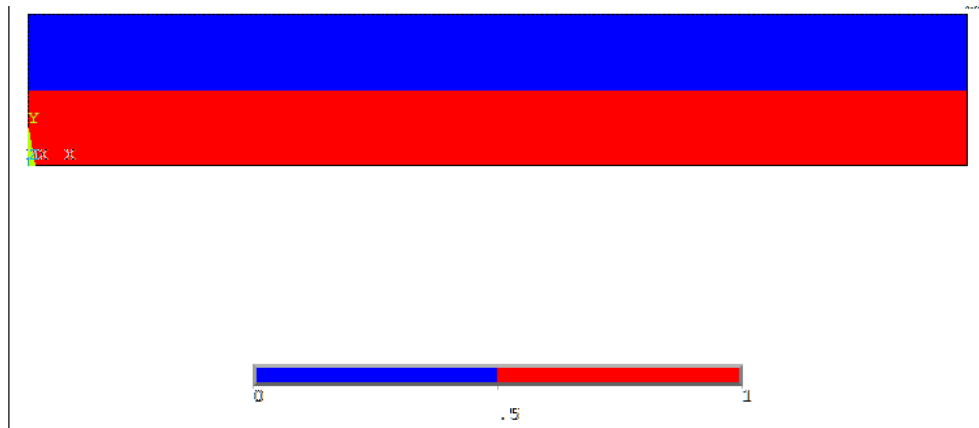
Figure 25: 2D planar Flotran model, Volume Fraction contour plot, initial location of fluid surface
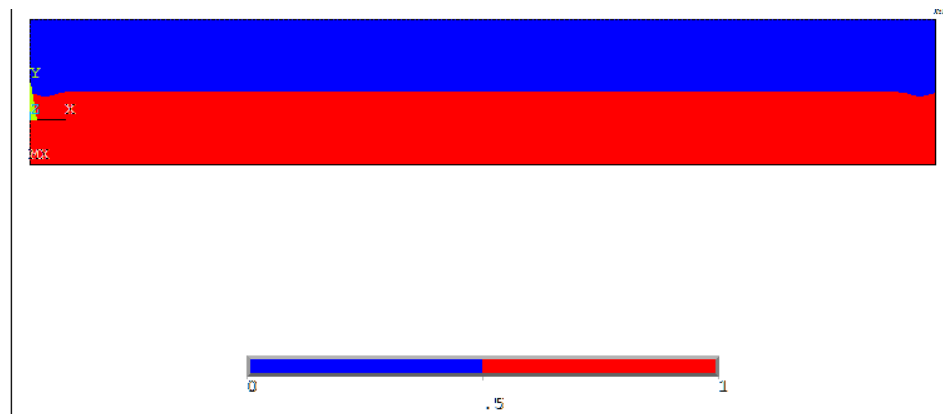
Figure 26: Beginning of wave development near outer free-slip boundaries
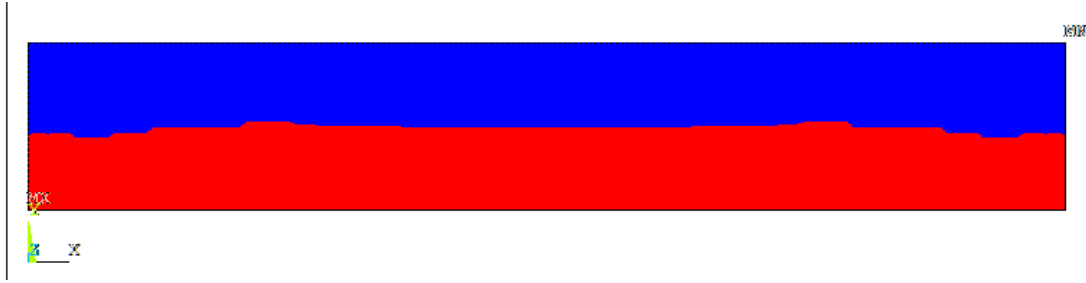
Figure 27: Waves propagating away from initial instabilities across fluid body
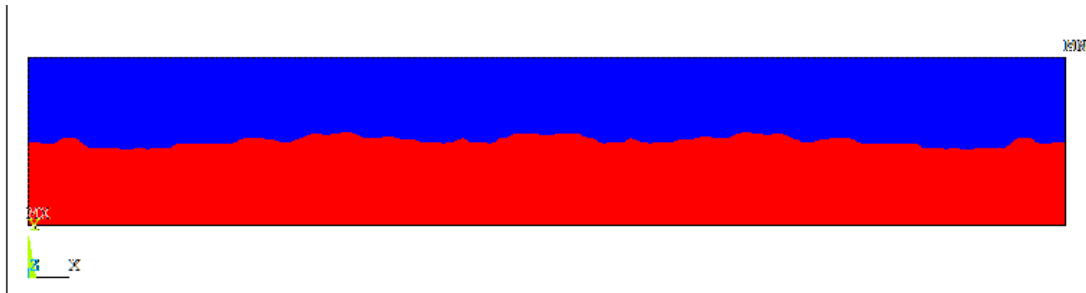
Figure 28: Full development of standing surface waves

Surface wave development is shown in Figures 26 and 27, and Figure 28 is an example of a model with fully-developed surface waves; frame-by-frame observation of single wave points on the surface confirmed that the surface of this system was responding at around 120 to 150 Hz, which is very close to the theoretically expected response of exactly half the driving frequency.

The next step in the process leading up to a model for critical parameter analysis was the implementation of axisymmetry, which would yield a model that better approximates a realistic three-dimensional fluid body. Once again, a time consuming trial-and-error method had to be used in order to generate a model with solution

convergence, which generally included minor time step adjustments and solution control settings unique to Flotran. The following screen captures (Figures 29 and 30) show that the model tends to oscillate at greater amplitude near its axis of symmetry, since lower frequency waves traveling from the outer edges will tend to meet at the center of a circular body and combine with the standing surface waves.
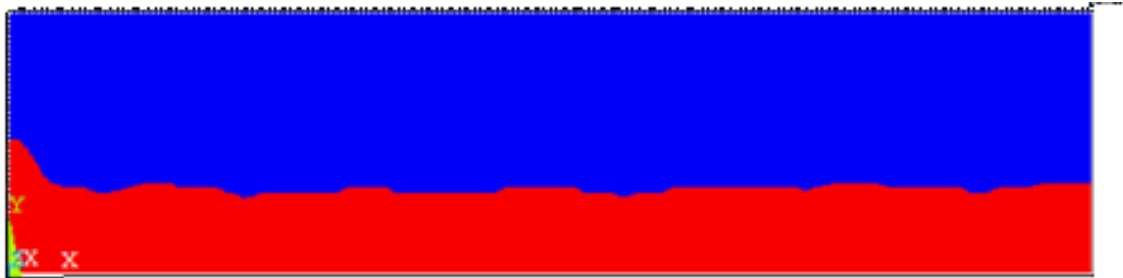
Figure 29: Peak oscillation displacement amplitude at axisymmetric boundary location, Flotran volume fraction contour plot

The next capture shows the center wave peak recoiling into a low point, with some disorder appearing in the valley due to the traveling waves oscillating at a frequency slightly different than the larger standing waves. The rest of the fluid surface appears to remain quite uniform in its oscillation.
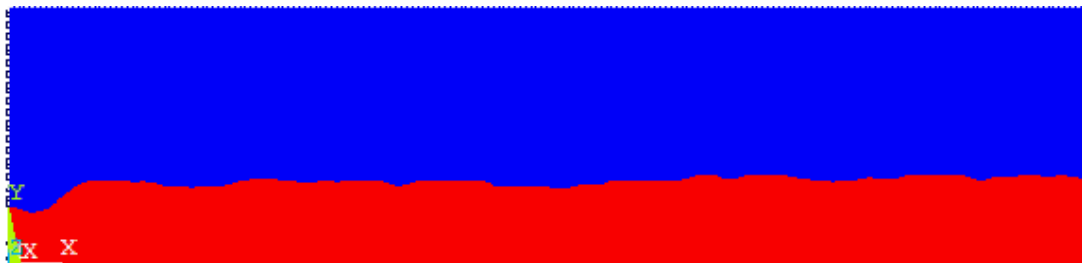
Figure 30: Valley of oscillation displacement amplitude at axisymmetric boundary location, Flotran volume fraction contour plot

In order to verify that the liquid surface is predominantly oscillating at half of the driving frequency, a series of screen captures of the 150 Hz model were observed in both volume fraction contour plot form and velocity vector plot form.
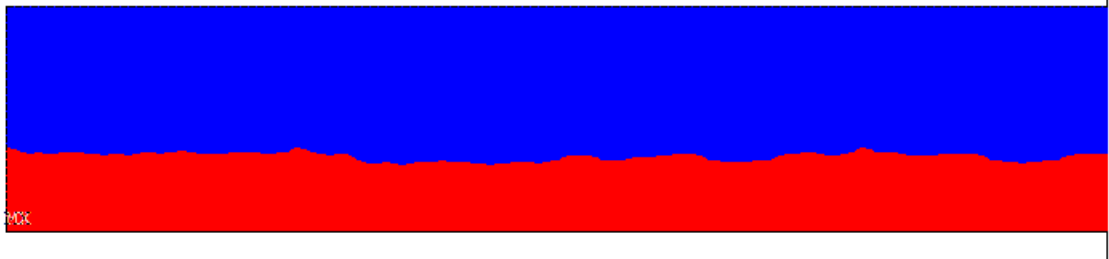
Figure 31: Time step 595, relative low displacement, Flotran volume fraction contour plot, 150 Hz case
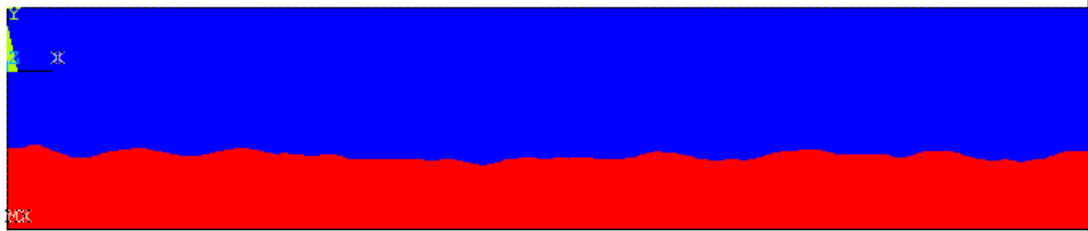
Figure 32: Time step 605, relative high displacement, Flotran volume fraction contour plot, 150 Hz case
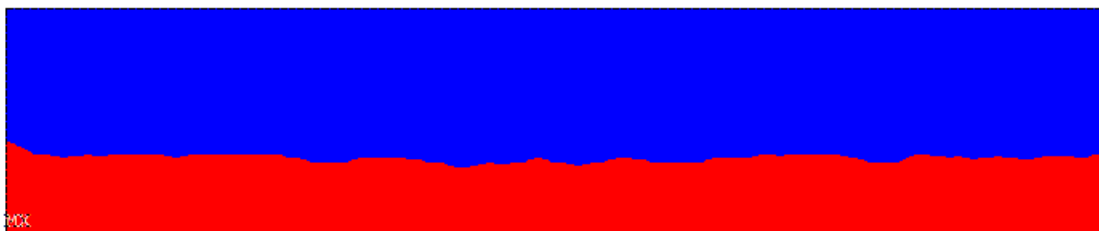
Figure 33: Time step 620, relative low displacement, Flotran volume fraction contour plot, 150 Hz case

This is difficult to observe in Figures 31, 32, and 33 due to the smaller waves traveling across the liquid surface from the horizontal reflection off outer free-slip boundary. However, a series of screenshots in

Figures 34, 35, and 36 showing velocity vectors describes the general state of motion of the surface more clearly.
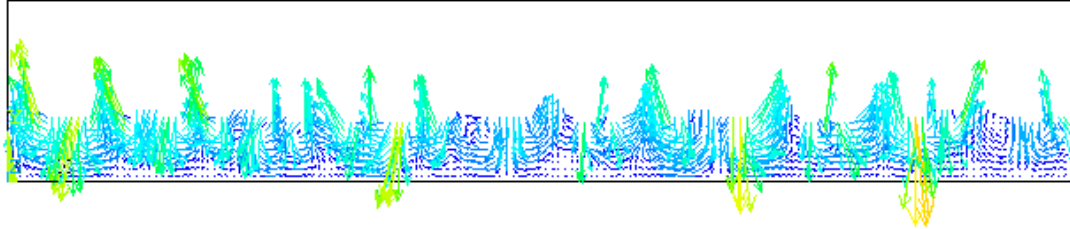
Figure 34: Time step 595, relative high velocity, Flotran velocity magnitude vector plot, 150 Hz case
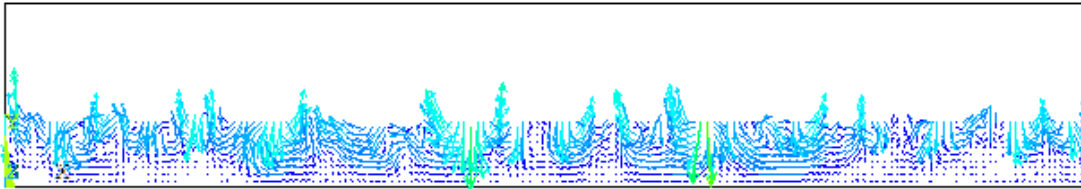
Figure 35: Time step 605, relative low velocity, Flotran velocity magnitude vector plot, 150 Hz case
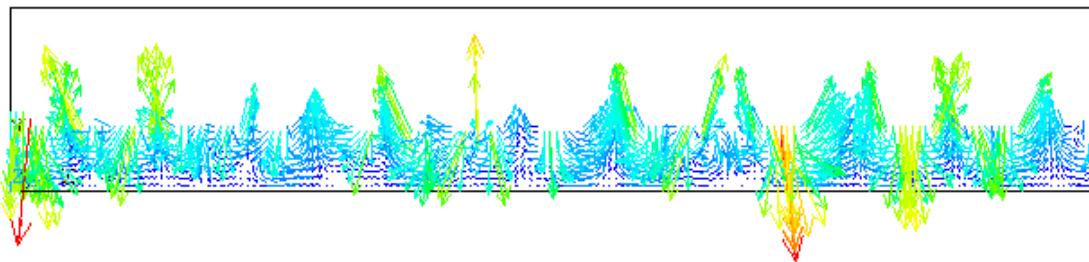
Figure 36: Time step 620, relative high velocity, Flotran velocity magnitude vector plot, 150 Hz case

The time period between these local maximums of velocity and corresponding local minimums of displacement is 0.0063 seconds. Doubling this value to account for a full wave oscillation period and taking the inverse yields a surface frequency of approximately 79 Hz, which is very close to the expected 75 Hz corresponding to a 150 Hz

base excitation (actuator). The slight discrepancy is likely due to recording results every 5 time steps rather than for each and every time step, which is done to reduce file size and disk write time.

Further, the expected wavelength for each case is verified by comparing the wave tips to an element plot of the same region. The region shown in Figure 37 is a close-up view of Figure 32, on the left side of the screen capture where clear, full wave tips have developed. The corresponding mesh plot provides an estimate of the size of the two consecutive waves according to the element edge length.
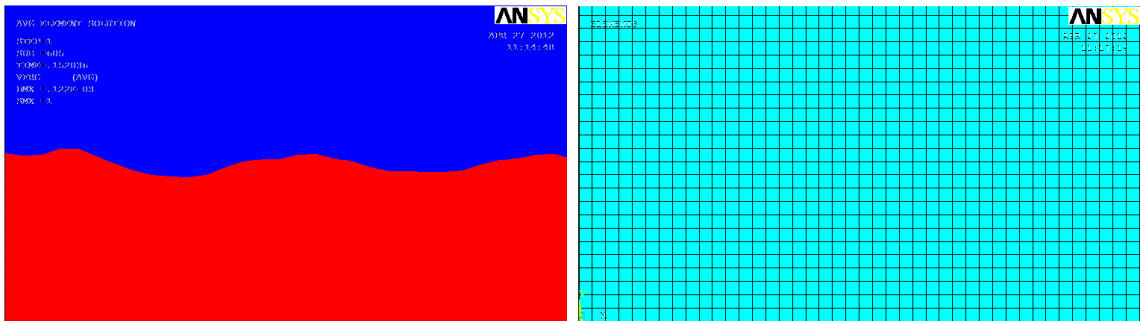
Figure 37: Time step 605, wavelength close-up and mesh comparison, 150 Hz case

There are 39 elements between the leftmost and rightmost peaks in the figure, which equates to a distance of 8.8 mm for the element edge length used in the 150 Hz case (215 μm). This means that each wave is about 4.4 mm in length, which is extremely close to the theoretical wavelength calculated to be 4.3 mm. Upon rearranging Equation 1 and solving for frequency, the surface is predicted to

oscillate at about 73 Hz, which again is very close to exactly half of the driving frequency.

Since the model appears to behave naturally based on what would be expected in a real system, further model verification steps can proceed for the analysis attributes including the mesh density (element edge length), the model size (body width in theoretical wavelengths), and the length of time steps. Most verification is done with the 300 Hz case due to the previously reviewed literature on a similar experimental system and solver run time requirements being minimized. High frequency ultrasonic cases require very small time steps and an order of magnitude more of them in order to reach a fully developed state.

The following set of figures are screen captures of velocity contour plots used for one of the model verification steps. The peak velocity data gathered for each CFD verification step and parameter test in the Results section is examined in this way.
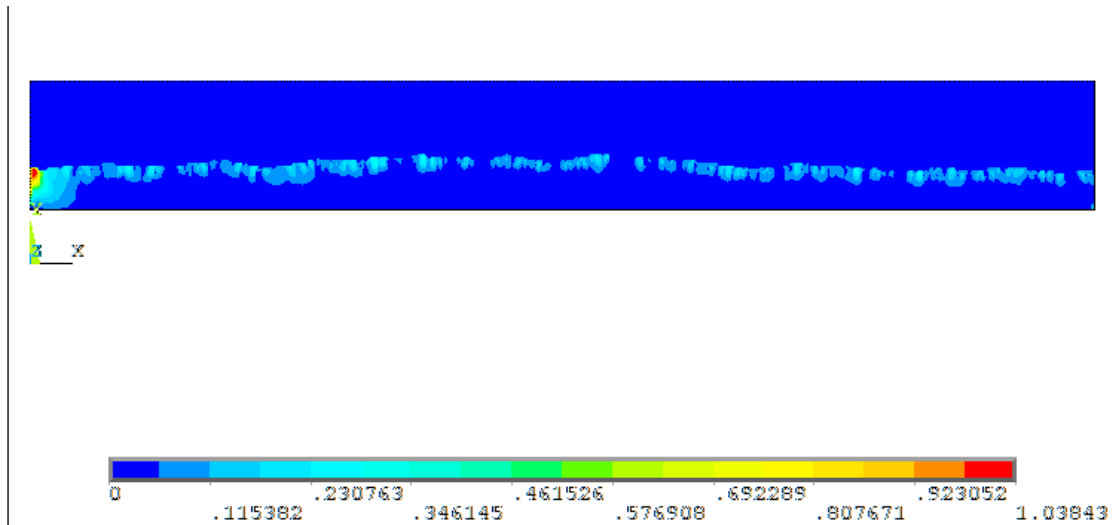
Figure 38: Flotran CFD contour plot, Y-component of fluid velocity,
screen capture near peak velocity time step
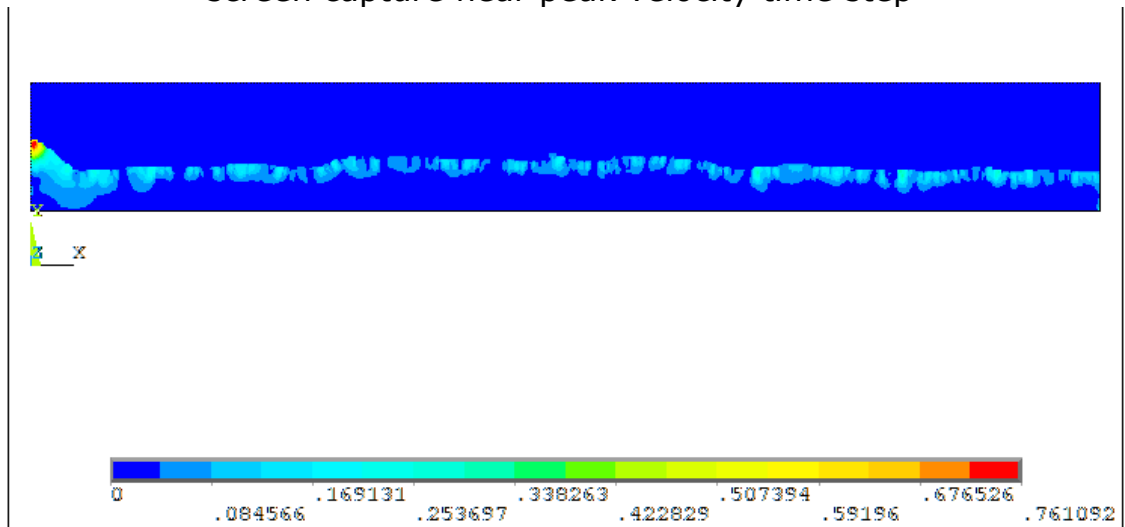
Figure 39: Flotran CFD contour plot, Y-component of fluid velocity,
resulting wave tip following velocity peak

For this particular model run, Figure 38 shows the central wave (red

spot on left side of contour plot) at the middle of its oscillation period

where it moving upward near the peak velocity developed in the run.

Figure 39 shows the resulting center wave formed as a result of this

peak velocity. The figure also gives an example of the approximate

size of a resulting droplet that is likely to initiate the atomization process for the entire surface. A length scale is not shown, but this wave tip is approximately 5 elements across between the axis of symmetry and the wave's inflection point. This distance represents a quarter of theoretical wavelength, so multiplying it by the element edge length (0.125 mm for the 300 Hz case) yields 0.625 mm, which corresponds exactly with the expected theoretical wavelength (2.5 mm). According to the energy balance theory and experimental work done, a droplet approximately 0.85 mm in diameter, or about a third of the theoretical wavelength, should eject at this point but it is believed that the Flotran solver cannot accurately model this behavior. However, the generated velocity can be used for model verification and parameter analysis. Thus, all further verification steps (model studies) and parameter tests will be based on an observational method of peak velocity analysis. A contour plot animation of the vertical component of velocity is created by ANSYS and the peak velocity occurring in the run is displayed as the maximum value in the velocity scale. Each clip is viewed independently, for each data point, to verify that the peak velocity recorded appears in the previously described expected location and with an expected wave shape.

The following minor sections describe the model verification steps taken to ensure that the system is behaving consistently. Each

model change is represented by a data point on a corresponding scatter plot.

Mesh Study

The mesh size was adjusted from the value corresponding to 20 elements across a single wavelength of response to less than half that size, which corresponded with the node limit on our ANSYS Academic license on an adequately sized model. The data is tabulated as element edge length in μm and maximum response velocity in meters per second; a scatter plot is shown in Figure 40. The data shows no trend in relation to mesh density and tends to average around 1 m/s for this particular system setup.
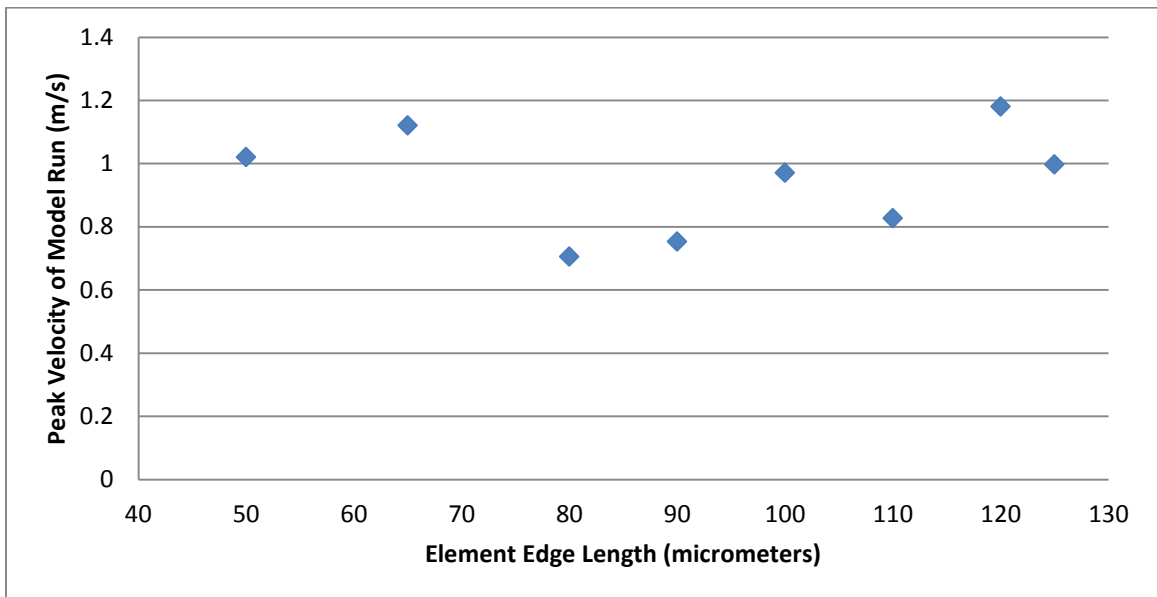
Figure 40: Flotran axisymmetric CFD verification, element edge length specified, peak velocities plotted for 300 Hz case

Model Size Study

As previously stated, the size of the model was tested to show at what point this parameter's influence is minimized. The model used for this portion of the study, like several other verification steps, was the 300 Hz case. Model size is taken to be the distance from the axis of symmetry to its outer wall (free slip condition), and is represented as a quantity of theoretical wavelengths given by Kelvin's equation. The data in Figure 41 shows that that a model size of approximately 20 theoretical wavelengths, which is what is recommended by ANSYS in general, will yield a conservative estimate of peak velocity achieved.
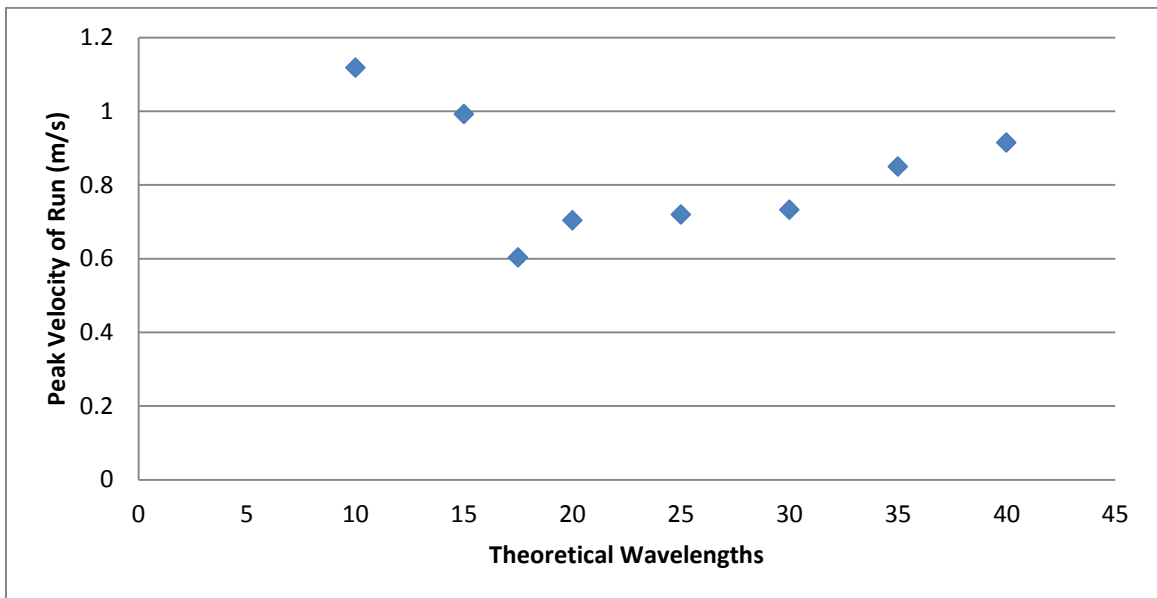
Figure 41: Flotran axisymmetric CFD verification, model size specified, peak velocities plotted for 300 Hz case

In this case (300 Hz), a model size of 20 wavelengths corresponds to an actual model width of 50 mm, which is roughly the size of the dish used in the laboratory experiments of Yule et al. Thus, all further tests

were carried out at a baseline of 20 theoretical wavelengths with minimal verification of larger or smaller sizes. All further testing proved that this size is a good conservative estimate and provides a relatively low solve time for all Flotran cases.

The following data in Figure 42 is for the model size of a 70 kHz case (ultrasonic), which was carried out briefly as a quick additional verification step.
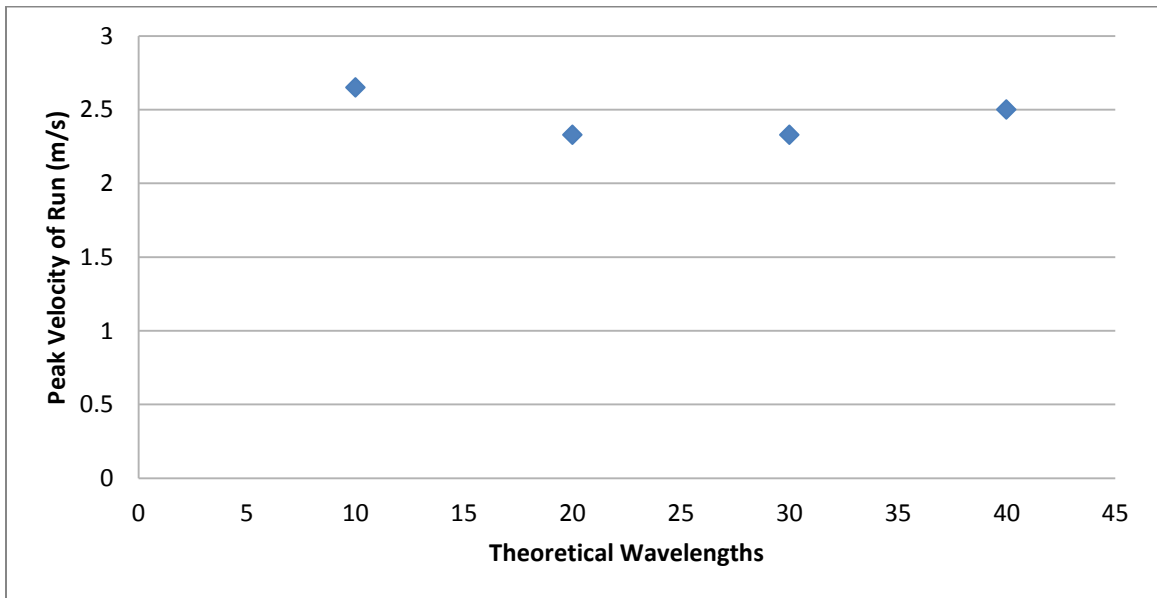
Figure 42: Flotran axisymmetric CFD verification, model size specified, peak velocities plotted for 70 kHz case

Further, a few more data points for model size were generated for the Omron's operating frequency of 178.6 kHz. The data in Figure 43 continues to show that 20 theoretical wavelengths is a very reasonable conservative estimate.
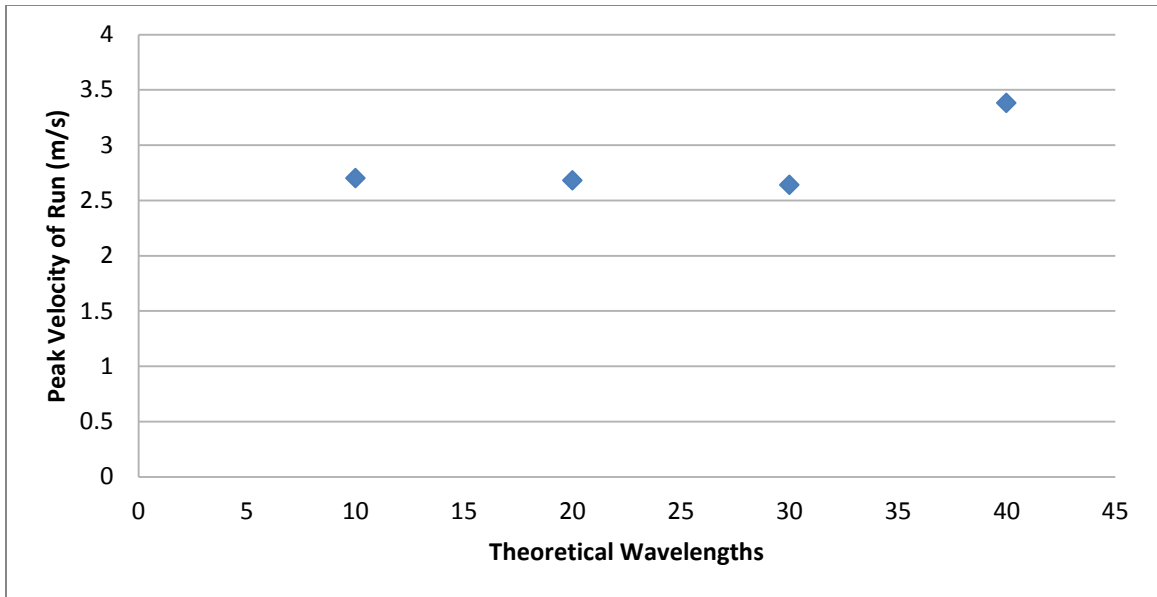
Figure 43: Flotran axisymmetric CFD verification, model size specified, peak velocities plotted for 178.6 kHz case

Time Step Study

Similar to the model size verification study, the time step length was tested to show its influence on the output of the system. This parameter was analyzed once again with the 300 Hz model and the time step to be tested was taken to be a fraction of the maximum allowable time step size. In the case of fluid flow, the largest time step size allowable for accurate results is the amount of time it takes a single "particle" of fluid to pass through one element, or from one node to an adjacent node. This quantity of time is calculated by dividing the element edge length (element size) by the maximum expected velocity in the system. The time step is analyzed at this maximum, then decreasing in 5% increments down to 50%. If a velocity higher than what is expected to develop occurs, reducing the

time step down to this minimal level would reveal the phenomenon. The data in Figure 44 shows that this does not occur and that the conservative model used is behaving as expected.
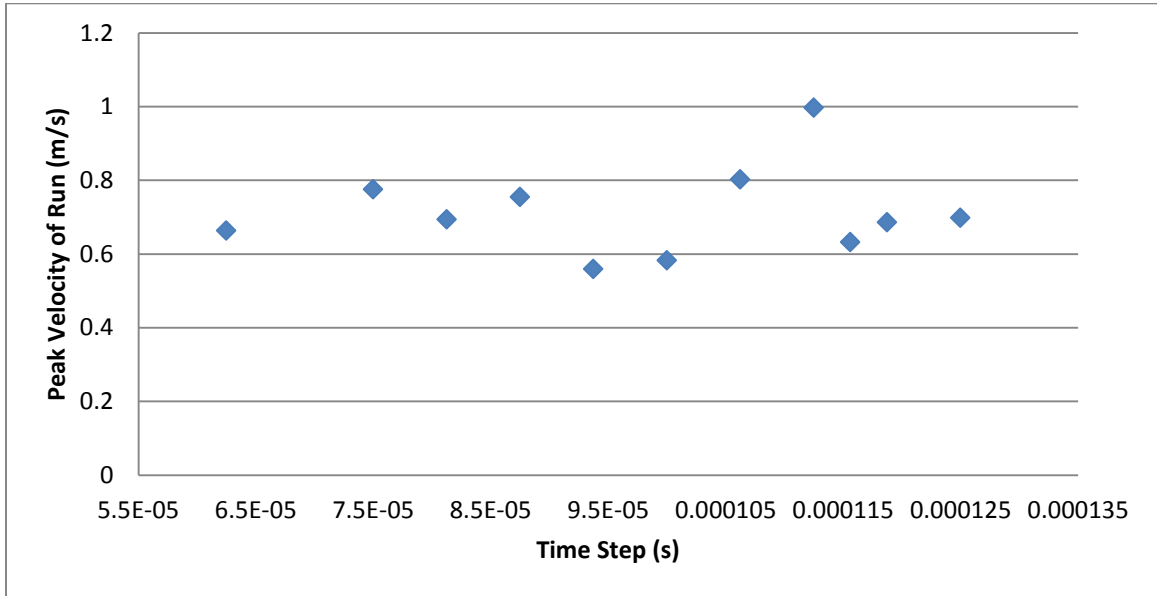
Figure 44: Flotran axisymmetric CFD verification, time step specified, peak velocities plotted for 300 Hz case

Low Frequency Parameter Analysis

As previously mentioned, the peak velocity data in this section is gathered in exactly the same way as the model verification steps. The difference is that the CFD parameters are decided upon and kept consistent while the system variables are altered in order to show trends. Element edge length is kept at 1/20th of a theoretical wavelength, model size is kept at 20 theoretical wavelengths across, and the time step is maintained as described in the previous sections.

Amplitude Variable

The interesting case of a 150 Hz, 0.13 mm displacement excitation system mentioned in the Literature Review has been analyzed in terms of its actuator amplitude. A spike in peak response velocity can be seen at the exact amplitude the previously mentioned study had photographed droplets ejecting at. The data in Figure 45 appears to be averaged at around 0.6 m/s except for a single anomaly. In order to verify that this was not simply a model error, the same code was run three times but the same peak velocity remained the final result. Identical code was used for the remaining data points, only altering the actuator amplitude value.
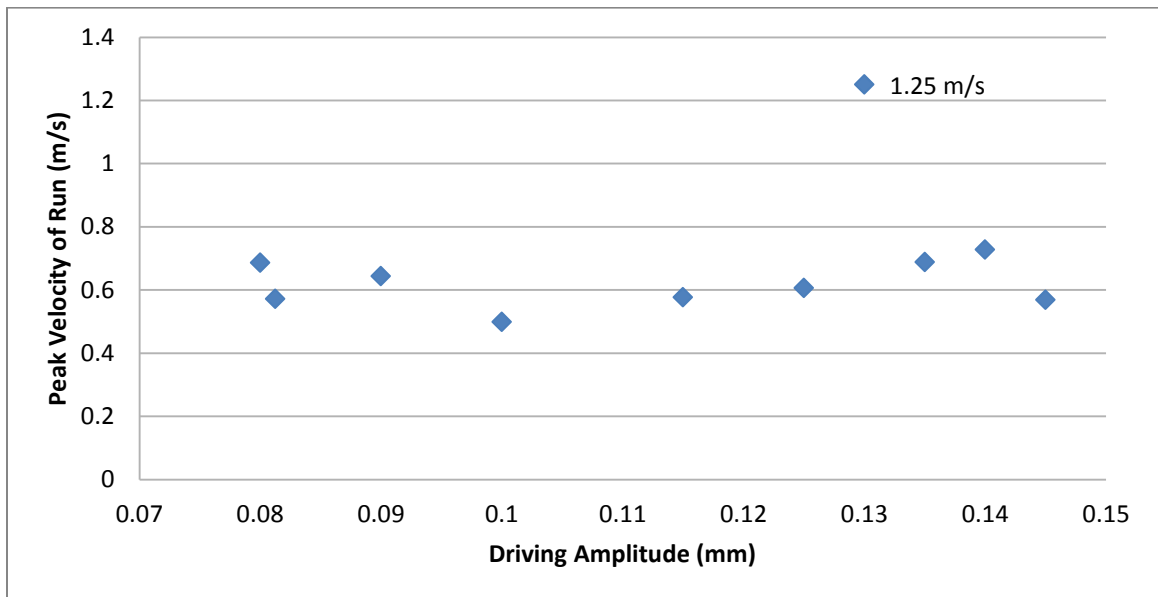
Figure 45: Flotran CFD parameter test, driving amplitude varied, peak velocities plotted for 150 Hz case

Driving amplitude testing was also carried out for the 300 Hz case; the velocity data is shown in Figure 46.
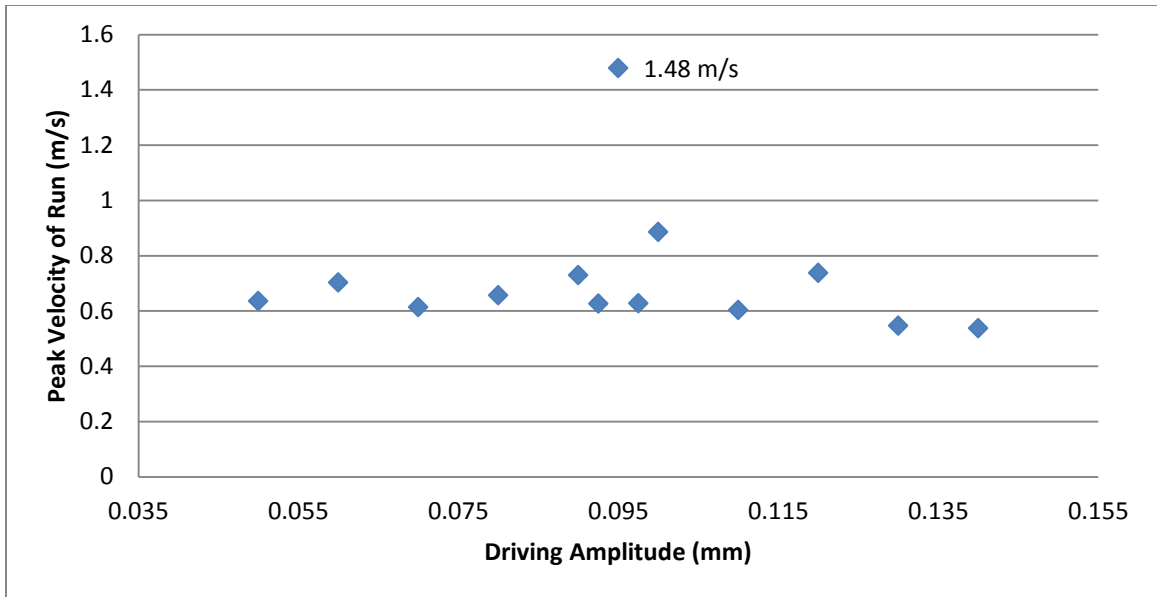
Figure 46: Flotran CFD parameter test, driving amplitude varied, peak velocities plotted for 300 Hz case

Once again, a very interesting data point was picked up during this portion of the study, except this time it did not correspond to the actuator displacement used in the experiments of Yule et al. However, the anomaly did occur very close to the quantity of 0.1 mm, and it is quite likely that an unexpected variation in the experimental setup caused this amplitude to be met during while tuning the device to generate atomized droplets. The data shows a spike at 0.095 mm displacement.

Depth Variable

The depth of the 300 Hz case was tested around the value reported to have been used by Yule et al. experimentally (2 mm). The increments in Figure 47 are 0.1 mm, except the two additional data points on either side of the spike.
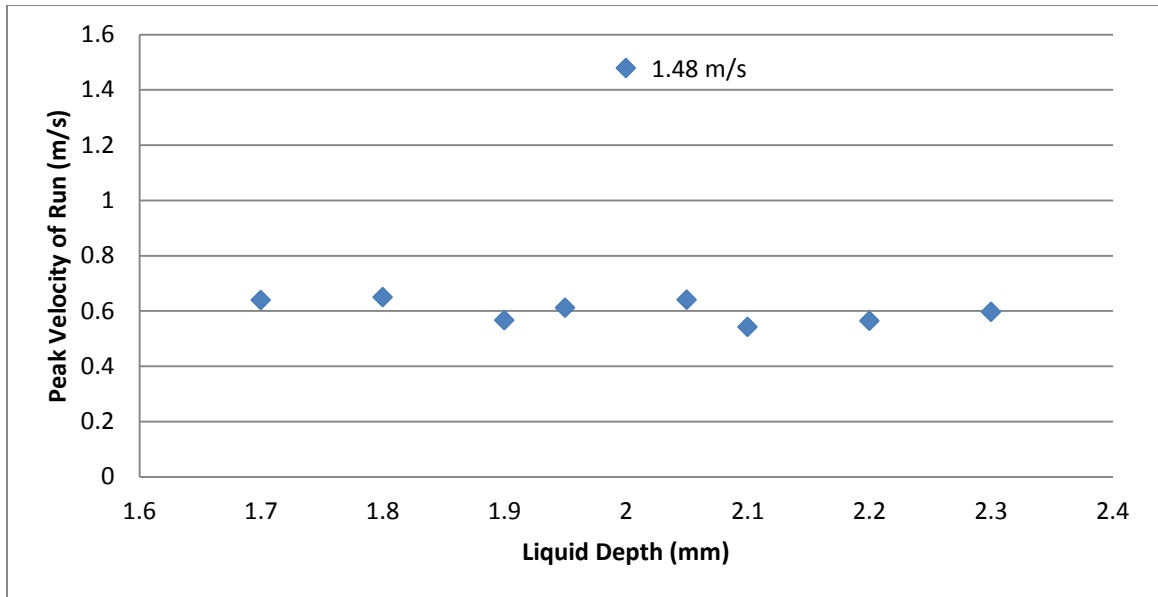
Figure 47: Flotran CFD parameter test, liquid depth varied, peak velocities plotted for 300 Hz case

Yet again, there is a spike at the experimental depth and no influence otherwise. It is important to note that the 300 Hz case data generated for Figure 47 was conducted at the displacement amplitude of 0.095 mm and that no velocity spike is observed for this depth test using 0.1 mm as the amplitude.

Frequency Variable

The 300 Hz case was tested to show the influence of driving frequency, with all other parameters remaining at the standard experimental values reported. To do this, the frequency was varied about the 300 Hz mark in 10 Hz increments, with a couple more data points added around the observed spike (Figure 48).
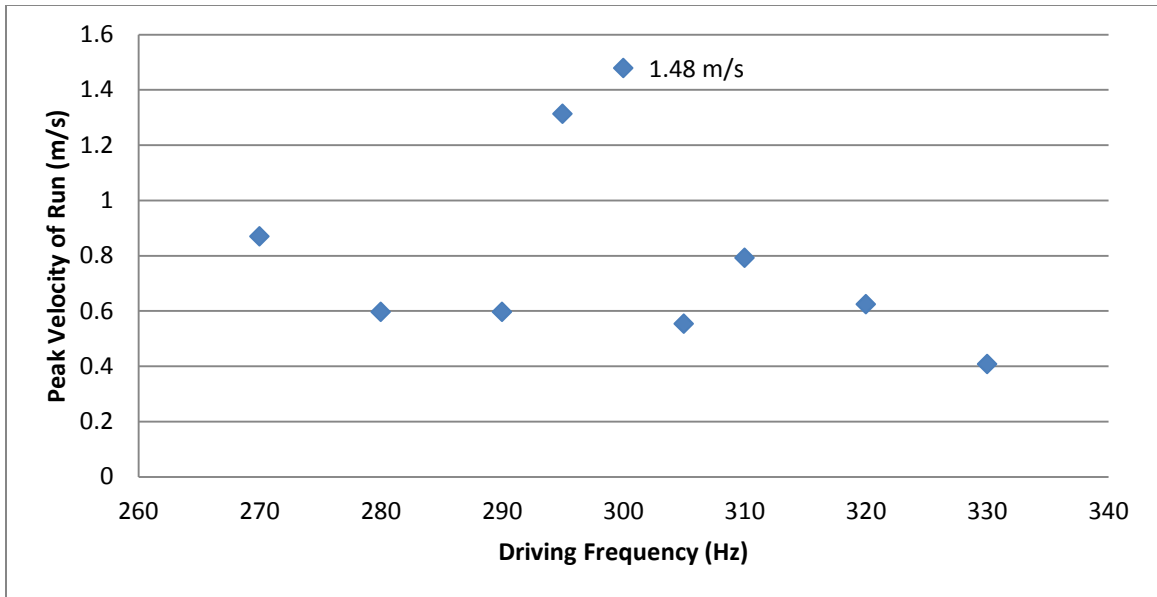
Figure 48: Flotran CFD parameter test, driving frequency varied, peak velocities plotted for 300 Hz case

Ultrasonic Parameter Analysis

For the 178.6 kHz case which simulates the conditions of the Omron Micro Air operating as a simple fluid atomizer, the following amplitude parameter test was conducted as the data describes in Figure 49. In this case, the peak velocity tends to average around 2.8 m/s except for a single value at 0.62 µm which surpasses 4 m/s. This increase is not nearly as dramatic as the low frequency cases and will be reviewed further in the Discussion section.
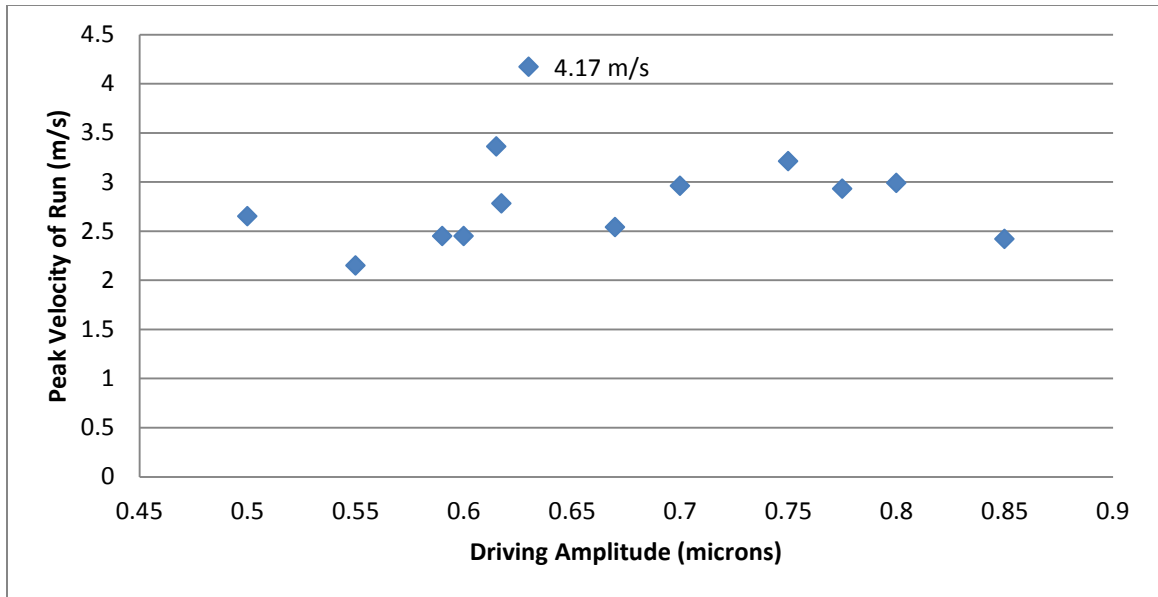
Figure 49: Flotran CFD parameter test, driving amplitude varied, peak velocities plotted for 178.6 kHz case at 25 micron depth

In addition, several runs of the Omron case (actuator amplitude of 0.8 microns) were conducted in an attempt to find the critical film thickness that would develop the same type of velocity spike present in the previously analyzed low-frequency models (data shown in Figure 50). No such spike was found, but the velocity tended to average around 3.2 m/s for models deeper than 20 µm. Convergence and size restrictions became limiting factors beyond 50 µm for the Omron case using a fixed time step, and it is possible that the critical depth lies beyond this point. More details on this can be found in the proceeding sections.
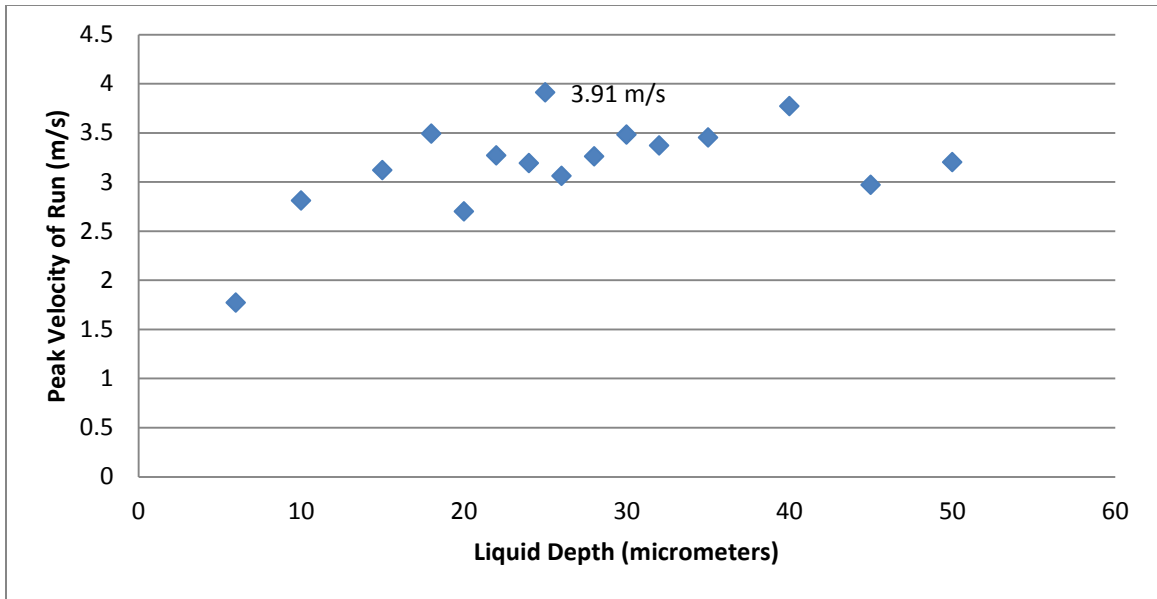
Figure 50: Flotran CFD parameter test, liquid depth varied, peak velocities plotted for 178.6 kHz case
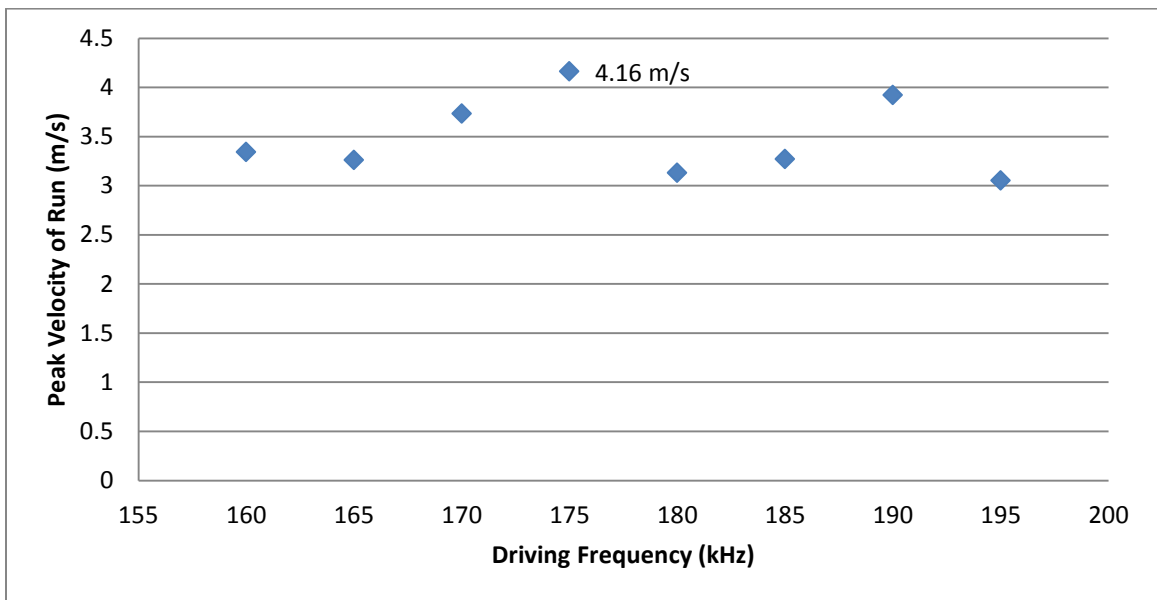
Figure 51: Flotran CFD parameter test, driving frequency varied, peak velocities plotted for 178.6 kHz case

Figure 51 shows data for the frequency parameter test conducted for the Omron case. The operating frequency of the model is varied within the range of 160 kHz to 195 kHz in 5 kHz increments

while keeping the amplitude and depth constant. The peak velocity generated averages at about 3.5 m/s and shows no trend or spikes.

CFX Solver

Capillary Wave Formation

The application of a periodic boundary condition made it possible to generate standing waves free of any edge effects, which resulted in a very uniform surface response. This also allowed the model to be analyzed at a size of 10 theoretical wavelengths, which was important for solve time concerns. Also interesting is that the surface wave pattern is clearly observed to be exactly 10 fully developed waves across (see Figure 54).

Several different cases were analyzed using CFX, including sonic (150 and 300 Hz) and ultrasonic (39.5, 70, and 180 kHz) models. They all tended to produce a similar surface wave pattern when operating in a stable manner, achieved through adjustment of boundary conditions and model parameters such as time step and mesh size or other solver variables and settings. Models operating unstable would "explode" immediately, or oscillate for several time steps before doing this seemingly at random. Figure 52 shows the initial fluid locations, with the lower region being the water portion. Figures 53 and 54 depict the wave formation in the model as it is run.

The surface waves appear to originate from some instability on or near the periodic boundary condition; it is likely that a localized physical instability may initiate surface wave formation in a real system.
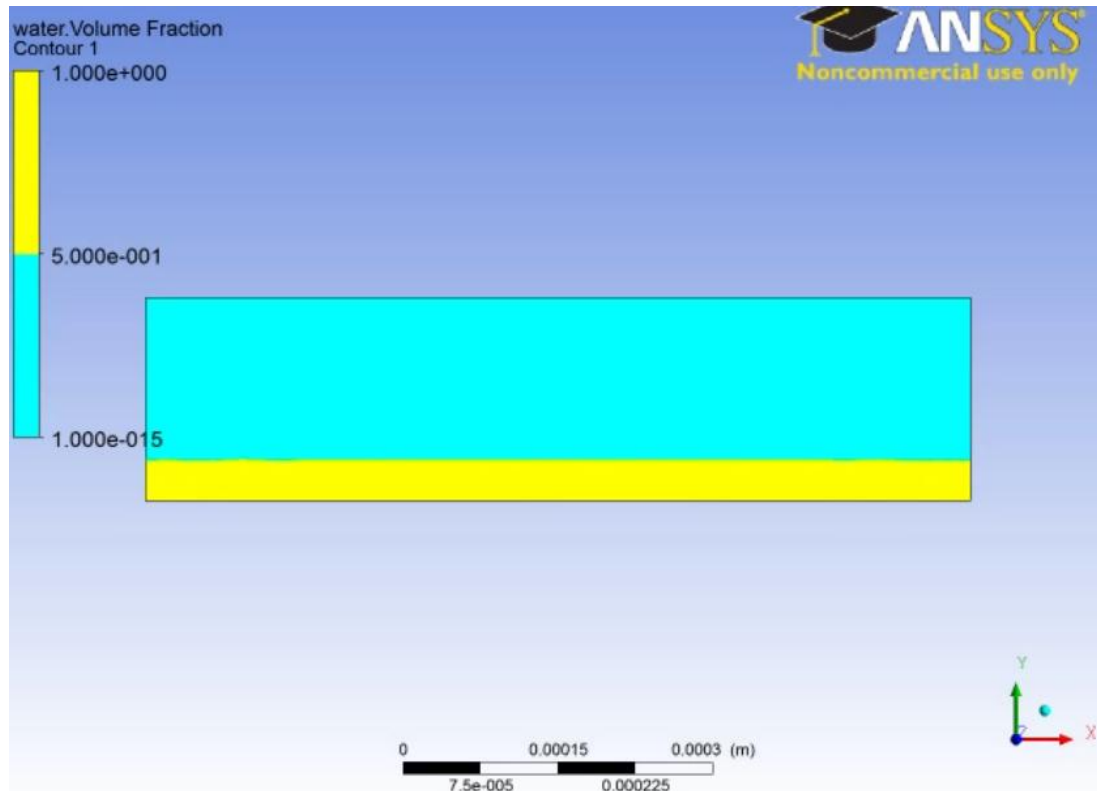
Figure 52: ANSYS CFX planar CFD model with periodic boundaries,
initial liquid location
(yellow is water, blue is air)

Figure 53: Standing waves beginning to form at boundaries and
propagate across fluid body, CFX
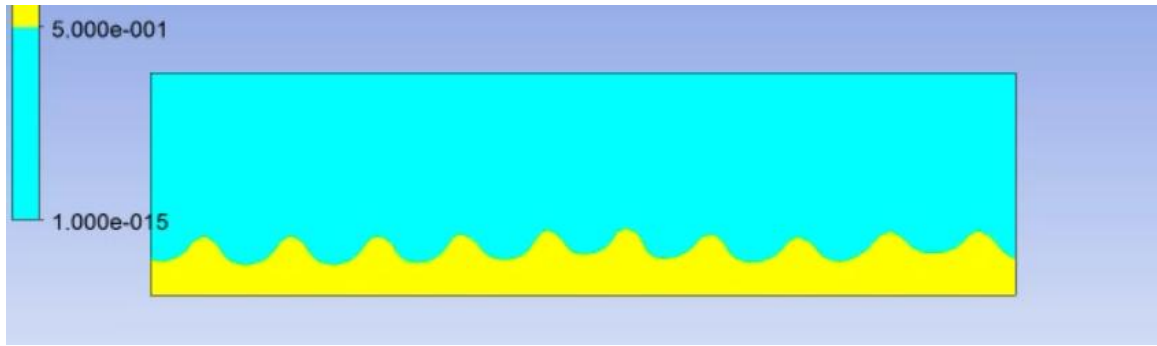
Figure 54: Fully developed, uniform standing wave pattern; CFX model

Much like the atomization process previously described, chain-reaction type events lead to quasi-steady state behavior in these oscillatory fluid bodies. This essentially means that predictable, stable behavior can originate from a seemingly random event or local instability.

Cavitation Model Dependence

The influence of cavitation was not studied at length with the CFX solver, but some effects were noted. At lower frequencies (sonic), toggling this model attribute on or off had no effect on the results or wave formation in general. However, at high frequencies (ultrasonic) the inclusion of cavitation bubble formation in the model acted as a sort of stabilization in the run; it is assumed that allowing the model to behave naturally removed the development of mathematical error resulting in divergence of the solution.

An issue which arose while using CFX is that the model would tend to "explode" before developing any kind of wave pattern. This

87

instability was usually observed as a large "tear" or void expansion in

the liquid portion of the model, which then proceeded to carry the

entire liquid region out of the analysis area very chaotically. This

could be explained as a divergence in the free surface solution in some

cases, but potentially relevant in others. Since the CFX models were

entirely set up using the ANSYS Workbench GUI, it seemed that

mistakes were easy to make compared to altering a few numbers in a

code file. Often an analysis would diverge after repeated attempts,

only to start from scratch and have it complete normally using

seemingly the same settings.

For the ultrasonic cases analyzed with CFX, the models would

often show very little surface oscillation before instability was reached,

either revealing actual phenomena or mathematical divergence.

Toggling the option for the development of cavitation bubbles in the

liquid had a stabilization effect which allowed some of these higher

frequency cases to generate a surface wave pattern in a predictable

manner.

Velocity Data

The models run in ANSYS CFX show a very predictable wave

pattern on the surface (when mathematical stability is achieved) which

is exactly the expected theoretical wavelength. However, the velocity

profile present in the contour plots of these runs is not fully

understood. What follows is an example of this situation, where a surface position which should correspond to a peak surface velocity shows the highest velocities occurring within the "air" region of the model. Figure 55 and 56 are captured at the same time step which coincides with the center of an oscillation period, or between wave amplitude peaks in a fully developed wave motion state.
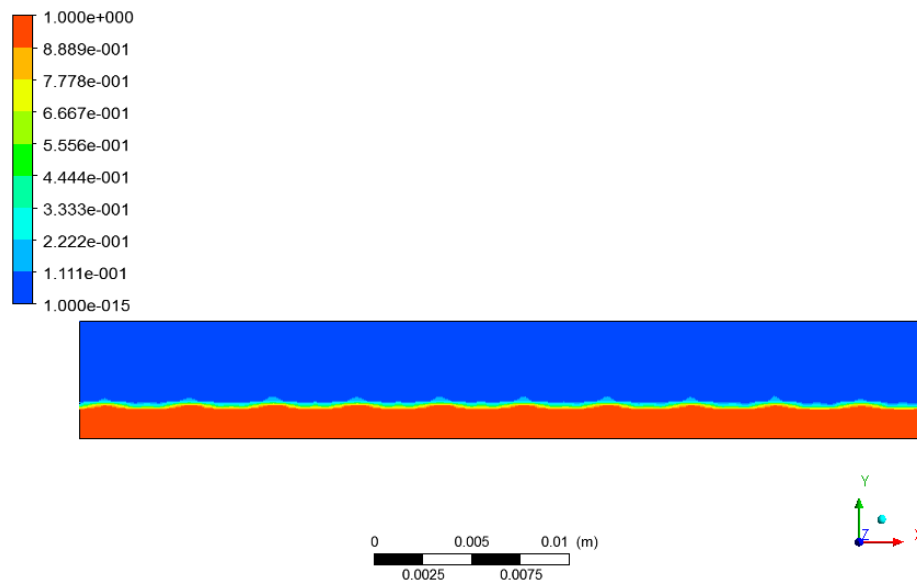
Figure 55: Volume fraction plot between oscillation displacement amplitude peaks, CFX 150 Hz case

Figure 55 is a volume fraction contour plot while Figure 56 depicts the velocity magnitude of the fluid defined as water only. What is shown in Figure 56 is interpreted either as noise in the results or some phenomenon which is not understood at the time of this writing. It is possible that liquid ejection of some form is only being shown as a velocity but not as a part of the volume fraction results. As previously stated, this is currently up for interpretation in this study.
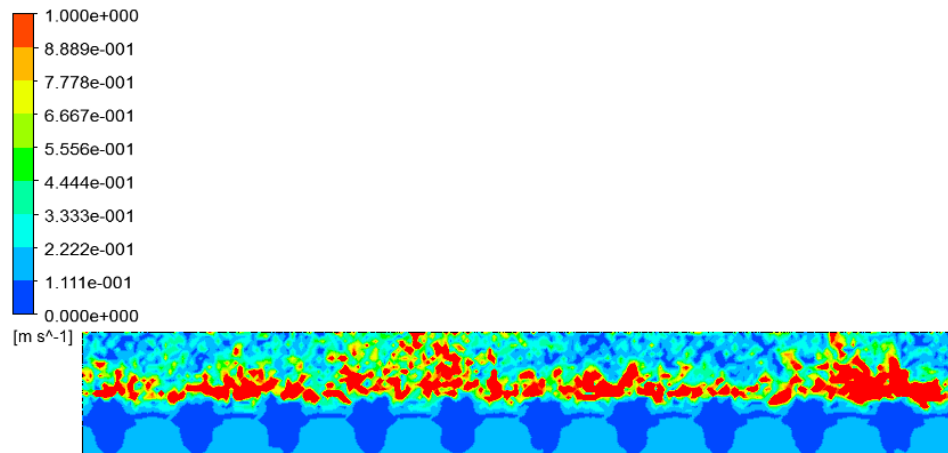
Figure 56: Water velocity magnitude plot at identical time step shown in Figure 44, CFX 150 Hz case

The CFX models differ from the Flotran models in that the influence of the surrounding atmosphere is assumed to be insignificant in relation to the generated results in Flotran, but it is required that an atmosphere region be defined in CFX. It is possible that certain specific attributes of the results generated in either solver are not valid for systems such as what is being modeled here, and it is well known that sound engineering judgment must be used when interpreting the results of any form of finite element analysis. Thus, the exact cause of this discrepancy is not known, but the data generated by Flotran for this study shows expected trends in initiating wavelengths and ejection velocity. The conclusions drawn about atomizing systems in the proceeding section will rely primarily on the Flotran results generated in this study for the previously mentioned reasons.

CHAPTER VII

DISCUSSION

Capillary Wave Properties

In order for a vibrating film of liquid to produce atomized

droplets, it is necessary that a few conditions are met. The first of

these conditions is that the film be deep enough such that the surface

can oscillate freely without interference from the actuating base on

which the film is held. Second, the actuator amplitude must be great

enough to excite the vibrating liquid surface to the point where the

peaks of the standing waves have enough kinetic energy to overcome

the resistant forces associated with the fluid interface. The quantities

of energy required for this threshold are largely determined by the

properties of the liquid, with surface tension being much more

influential than viscosity for water and water-based liquids (like most

medications). Surface tension is the primary resistance to droplets

escaping the surface of the liquid medication film and it also plays a

major role in determining potential droplet size. Higher surface

tension leads to longer standing wavelength, which the mean droplet

diameter is proportional to. While raising the droplet size for a given

actuating frequency increases droplet kinetic energy, it also increases the resistant energy acting upon it. It follows that the final condition to be met coincides with the previous condition, that the liquid's properties are conducive to generating atomized droplets for the given operating setup which includes film thickness (depth) and actuator amplitude as primary factors.

The vibrating film depth must be sufficient to support surface oscillations; this quantity is generally on the length order of the standing waves produced. This basically means that a wave "aspect ratio" of about one-to-one is necessary in order for the surface to oscillate freely. This means that a fully developed wave's length will correlate closely with its critical peak height, which should be a smaller quantity than the film thickness. Films that are an order of magnitude smaller than the length of an expected standing wave will simply not begin to oscillate, and will "ride along" with the actuator or be flung off entirely in bulk form. If a vibrating film produces atomized droplets at a given depth, increasing this depth beyond a certain threshold will lead to sporadic droplet production and increasing it further will lead to excessive damping in the system which halts the process entirely.

For a given liquid film or body depth, a certain range of actuator amplitude will result in surface oscillation leading to atomized droplets. Below this range, surface vibration may not occur and above it, bulk

motion of the fluid body will occur and no atomization will result. It is entirely possible that certain systems will not have critical actuator amplitudes and will either fail to produce surface waves, or will simply experience bulk motion of the liquid body. Such systems are beyond the scope of this research.

A distribution of droplet sizes exists in all standing wave atomizers which implies that droplets significant larger than the mean size are produced. As droplet size increases, kinetic energy increases along with resistant energy but kinetic energy increases more quickly due to the nearly spherical shape of an ejecting droplet. Thus, larger droplets on the distribution will tend to initiate the atomization process while destabilizing the entire liquid surface in a sort of chain-reaction.

Low Frequency Energy Balance

Surface Velocity

Under the conditions described by Yule et al, the case of 300 Hz generates a peak velocity of 1.48 m/s using the previously described CFD free-surface method. An exception to the conditions described in the literature is that a 0.095 mm actuator amplitude is used instead of 0.1 mm, but such a small discrepancy is thought to either be experimental error or caused by random variation in the experimental conditions, the reporting of said conditions or their interpretation. Whatever the reason may be, this only represents a difference in the

actuator amplitude that is 0.005 mm or 1/200th of 1 mm, or 5% of the measured actuator amplitude. The case of 150 Hz generates a peak velocity of 1.25 m/s at 0.13 mm actuator amplitude, which is the exact quantity reported for the experiment so no further explanation is necessary.

The most important piece of information to take away from the current study is that of the compelling evidence of a tuned system for each of these cases. The CFD analysis shows that a relatively wide range of actuator amplitude can be used with little change in the peak velocity generated in the system. Of course, the exception is that one particular value of actuator amplitude effectively doubles the velocity generated in the system. This marked increase in kinetic energy occurs at exactly the conditions used for past experimental analysis and only at this specific set of parameters. This set of parameters, which includes the liquid depth, actuator amplitude, and actuator frequency, coincides with a quantity of kinetic energy which significantly surpasses the resistant energy of the liquid surface.

The following table shows several values from the 150 Hz actuator amplitude CFD parameter analysis and their corresponding peak velocities compared to the threshold velocity of 0.77 m/s for an ejecting droplet of this case's mean diameter, which is calculated to be 1.5 mm.

Table 1: Energy Comparison of Peak Velocity Generated in CFD Run to Threshold Velocity (0.77 m/s) of 150 Hz case, Mean Droplet Diameter of 1.5 mm

Actuator Amplitude, mm	Peak CFD Velocity Generated, m/s	% of Required Kinetic Energy
0.090	0.643	70.1
0.100	0.498	42.0
0.125	0.606	62.3
0.130	1.250	265
0.135	0.688	80.2
0.145	0.568	54.7

Table 2 is similar to the previous table, except it shows values from the 300 Hz actuator amplitude CFD parameter analysis. In this case, the threshold ejection velocity for a droplet of mean diameter (approximately 0.92 mm) is 0.97 m/s.

Table 2: Energy Comparison of Peak Velocity Generated in CFD Run to Threshold Velocity (0.97 m/s) of 300 Hz case, Mean Droplet Diameter of 0.92 mm

Actuator Amplitude, mm	Peak CFD Velocity Generated, m/s	% of Required Kinetic Energy
0.060	0.703	52.7
0.080	0.656	45.9
0.090	0.729	56.7
0.095	1.48	234
0.100	0.886	83.8
0.120	0.738	58.1

The critical amplitude of these cases is highlighted in green and clearly shows the excess kinetic energy resulting from the doubling velocity present in their respective unique parameter configurations.

Droplet Ejection

At the mean droplet diameter, the Flotran CFD analysis shows that the 150 and 300 Hz cases generate enough velocity to eject

droplets according to the energy balance in Equation 9. These cases are likely to generate a very uniform surface wave pattern and a corresponding droplet distribution that is more tightly centered on the mean droplet diameter than an ultrasonic case due to a reduction in random disorder. Specifically, the 150 Hz case generates 265% of the energy required in wave tip kinetic energy to overcome surface resistance. Such an excess of wave tip velocity and corresponding kinetic energy is possible only in low frequency cases of considerable liquid depth and low actuator velocity. As frequency increases, required film thickness decreases as the actuator velocity increases substantially which gives a much higher potential for bulk motion of the vibrating liquid body. Similarly, the 300 Hz case used for most of the verification purposes generates 234% of the required kinetic energy for droplet ejection at the mean droplet diameter. Excesses such as those mentioned may be required to successfully carry the ejected droplet away from the vibrating surface since drag and gravity has more of an effect on the larger droplets produced in these low frequency cases.

Ultrasonic Energy Balance

Surface Velocity

Since the actuator amplitude of the Omron Micro Air is measured to be 0.8 μm at 178.6 kHz in the experimental section, varying the

film thickness yielded a peak velocity of 3.91 m/s at 25 μm depth.   At this depth, modifying the actuator amplitude to 0.62 μm yielded a slight increase to 4.17 m/s peak velocity. According to the energy balance requirements, to eject a droplet of the mean diameter for this case (13.1 μm) a peak velocity of 8.22 m/s would need to be generated in the CFD run.

An increase to the required velocity under the Omron's operating frequency represents a change similar to what is found by optimizing the amplitude and depth conditions of the low frequency cases. Based on the information that is currently available, it is only reasonable to expect that this optimized system is specified correctly by referencing what is believed to be an existing "tuned" system. It is expected that the correct configuration of parameters would result in at least a doubling of the peak velocity generated in the CFD run, which would indicate a system which overcomes the resistant energy of the liquid surface and produces atomized droplets. This specific configuration was found to exist for the low frequency cases and is expected to exist for the ultrasonic cases. The exact configuration was not found in this study, but the fact that such conditions may exist for this type of system should be taken as its primary success.

To further illustrate this point, near the end of this writing, an automatic (solver controlled) time step specification in Flotran was

implemented instead of a fixed time step, which is what is used for the rest of the solver runs. This allowed deeper models to converge more easily for the Omron's ultrasonic (178.6 kHz) case. A slightly higher velocity was generated in one of these model runs, but not to the extent of revealing appropriate kinetic energy levels for atomization initiation.
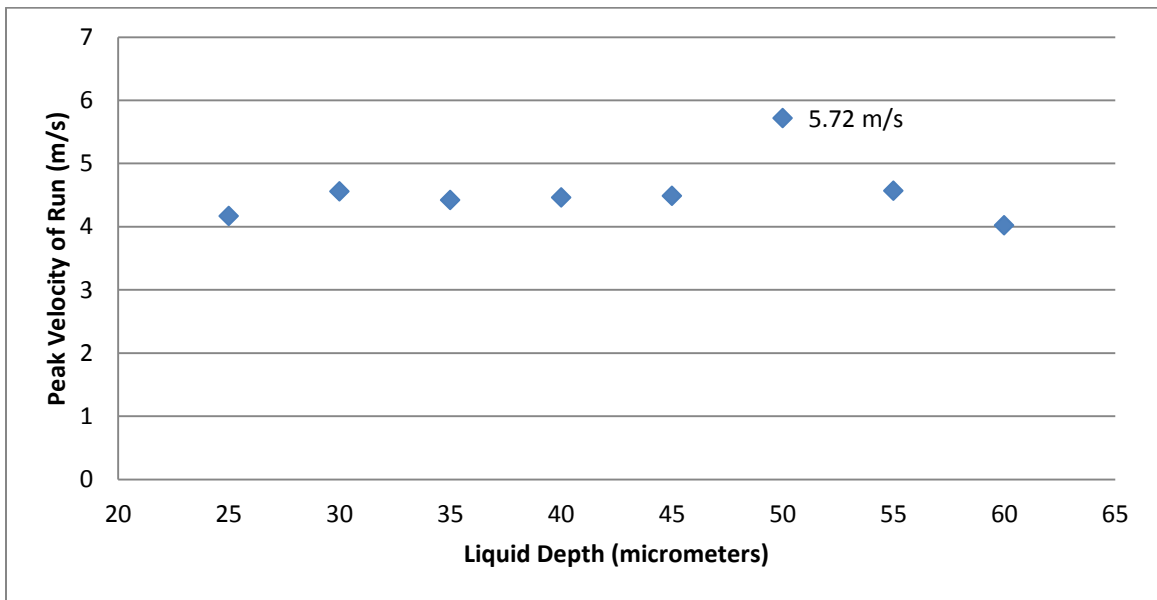
Figure 57: Automatic time stepping, liquid depth varied, peak velocities plotted for 178.6 kHz case

This further increase gets closer to the required peak velocity and generates 48.4% of the kinetic energy needed to overcome the surface resistance for a droplet of mean diameter, which occurs at the labeled data point of 5.72 m/s at a liquid depth of 50 μm.

Size Distribution Considerations

The proceeding discussion topic is not as well supported as previous assertions; however, it ties in the droplet size distribution to

the ultrasonic cases as a way to potentially explain how such atomizing conditions can initiate. This distribution is difficult to measure and may vary significantly from case to case, but using the aforementioned references as a guideline it may point future studies in the right direction and nearly provides support for the work done in this study.

According to the droplet size distribution for the Omron Micro Air shown in Figure 18 (Chapter 4), it is observed that if a 3 μm diameter droplet exists at a probability density of approximately 1.5%, it is equally likely that a droplet 23 μm in diameter exists simultaneously at the same probability density. The curve clearly shows that even larger droplets have a relatively high probability of being generated, but for the sake of this discussion it is reasonable to match the large droplet's probability density to one that the Omron device is documented to produce. It is likely that a larger droplet may initiate the process of atomizing droplets and as previously stated, the orifice plate may act as a screen for these larger droplets to be extruded through and broken up or enough of the smaller droplets are generated such that a sufficient flow rate of these droplets is allowed to pass through. For the Omron conditions, using the calculated mean droplet diameter of 13 μm, the system only generates 48% of the kinetic energy required for droplet ejection at the maximum velocity found for this case (5.72 m/s). However, if it is assumed that a droplet of 25 μm diameter

initiates the process, this peak velocity generates 90% of the required kinetic energy for overcoming the surface resistance. If a parameter configuration is found which results in only a small increase in generated velocity compared to the low frequency cases, this "initiating" large droplet would overcome the ejection resistance and begin the chain reaction leading to a fountain of atomized droplets.

CHAPTER VIII

RECOMMENDATIONS

Further Experimental Verification

In this study, the measurements of the Omron Micro Air's

actuator are taken only when the device is operating under minimal

loading conditions. While atomizing liquid medication through the

vibrating mesh, the actuator is loaded by this fluid and also by the

vibrating mesh itself. It is believed that the operating frequency is not

significantly altered due to an increase in load according to the

characteristics of a vibrating piezoelectric crystal and its voltage

source, but it is expected that the amplitude of vibrating is reduced

under load. This reduction in transmitted power to the liquid and

vibrating mesh is suspected to be a relatively low fraction and

significantly less than an order of magnitude. However, the change in

amplitude may be very significant to the effectiveness of the device in

producing atomized droplets. The results generated in the CFD

analysis portion of this study show that for systems of known

atomizing conditions, there is only one extremely narrow range of

actuator amplitudes which will produce standing wave tip velocity

sufficient to exceed the fluid surface resistance. Also, this narrow

range of actuator amplitudes only corresponds to a specific liquid film

thickness, which is another quantity that is difficult to measure while

the Omron device is operating. In general, a more extensive

experimental analysis of this device is necessary in order to fully and

properly model its parameters and behavior in a CFD analysis. The

incredibly small range of variables which determine whether or not a

vibration-induced atomizing system operates is the primary concern

following this study; had this discrepancy been discovered earlier in

the process of conducting this research, more work would have done

in this specific area in order to generate more conclusive findings for

the ultrasonic frequency cases.

Since the Omron device was observed to produce a small "puff"

of atomized droplets when operating with only a small volume of water

on the tip of its actuator and without the mesh it place, a crucial

question arises; if only a specific configuration of parameters is able to

initiate atomization according to the CFD analysis, why is it that such a

wide range of film thicknesses apparently generates atomized particles

of water? The range referenced here is from an amount so small that

it only covers approximately 50% of the actuator tip surface to an

exactly covered actuator tip, corresponding to approximately 0.5 mm

to 1 mm of fluid depth, respectively. A potential explanation for this

phenomenon is that such a small liquid body has a curved surface due to the surface tension interaction with the stainless steel actuator tip, and that a chain reaction occurs from a region of fluid at the critical depth or some other unknown nucleation site associated with ultrasonic frequency cases. High speed photography may be able to shed light on these effects.

Another interesting test would be to generate continuous atomization through a membrane other than the metal orifice plate. A sheet of fabric or plastic with similarly-sized openings could be mounted above the actuator and potentially adjusted to allow the micron-scale droplets to pass through it. It is unknown if this setup would allow for a continuous plume to be generated by the device or if the metal mesh plate is integral to this function.

Initially, experimentation with the circuitry of the Omron device was planned for this study but was never carried out. Relevant tests would include varying of the amplitude and oscillation frequency of the actuator similar to the parameter tests carried out in the CFD analysis to document any similar trends. In addition to a test such as this, and perhaps more importantly, an experimental setup should be devised which mimics the low frequency arrangements described in the documented past literature and also the CFD models. From there, the CFD model could be refined and checked for correlation with the

ultrasonic frequency cases. Even if achieving the correct parameter combination for atomization proved to be very difficult at the Omron's normal operating conditions, the system could simply be tweaked in terms of frequency and amplitude until droplets were produced. The CFD model could then be easily altered to reflect the experimental setup were a "sweet spot" was found.

3D CFX Model

The ANSYS CFX analyses produced some very interesting results for the amount of time spent refining the models for this particular study. The advanced features of this software could allow for the generation of a model which actually displays droplets being flung from the liquid surface if the time was taken to thoroughly understand the code and its limitations. A major problem encountered while working with these models for this study is that a true axisymmetric analysis is not possible in CFX, at least to the author's knowledge. Thus, rough representations of the model using 3D elements were the only achievable methods. An appropriately meshed, fully sized and dimensioned 3D model could be run at the expense of a significant amount of computing resources. Analysis on a powerful computing cluster or multi-core solver may be necessary for the analysis to finish in a reasonable amount of time (taking into account the computing power and speed available in production systems at the time of this writing).

2D/3D Fluent Model

Fluent CFD is another highly respected code used for countless types of fluid simulations. However, a model implementing this software was not able to be generated in the time available for this study due to its complexity. Nearly every available CFD concept at the time of the software's release can be implemented in this solver, but this great potential power often precludes the aforementioned difficulty of operation and as such, a very thorough understanding of CFD and Fluid Mechanics is necessary to generate a working model. Beyond the vast breadth of parameters available for modeling, both 2D and 3D modeling capabilities exist in Fluent. It follows that the atomizer concept could be developed in 2D (axisymmetric) to take advantage of the inherent computational efficiency of this type of model, which could then built up to a full 3D analysis to visualize and measure the formation of spherical droplets and fully defined surface waves.

In addition to solving the problem the problem itself with a more advanced model, much could be learned about the nature of CFD models in this configuration and how certain parameters apply to the relatively simple Flotran code. Because Flotran models are so simple and run very quickly, parallels could be drawn between the more advanced solvers and this one in order to accelerate the development of optimized atomizing systems.

APPENDICES

Appendix A

ANSYS Code

150 Hz Case (sample)

```
FINISH
/CLEAR
/TITLE,150_13
/PREP7
!*
!***LIQUID FILM DIMENSIONS***
DEPTH =  0.002
RADIUS = 0.0043*20
!*
!***MESHED AREA***
HEIGHT = DEPTH*3
MSHSIZE = 0.0043/20
!*
!***OPERATING CONDITIONS***
FRQC = 150
AMPLI = 0.00013
!*
!***TIME STEPS***
STPS = 2000
STSIZE = MSHSIZE/0.77*0.90
!*
!***ELEMENT TYPE***
ET,1,FLUID141
!*
!***OPTIONS***
!*
KEYOPT,1,3,1      ! SYMMETRIC ABOUT Y (YES = 1)
KEYOPT,1,4,1      ! ALLOW MESH MOTION
!*
!***GEOMETRY***
RECTNG,0,RADIUS,0,HEIGHT
!*
!***MESH***
ESIZE,MSHSIZE
AMESH,ALL
!*
!***SOLUTION OPTIONS***
!*
FLDATA1,SOLU,TRAN,1
FLDATA1,SOLU,FLOW,1
FLDATA1,SOLU,TEMP,0
FLDATA1,SOLU,TURB,0
FLDATA1,SOLU,COMP,0
FLDATA1,SOLU,VOF,1
FLDATA1,SOLU,SFTS,1
FLDATA1,SOLU,IVSH,0
FLDATA1,SOLU,SWRL,0
FLDATA1,SOLU,SPEC,0
FLDATA1,SOLU,ALE,1
FLDATA1,SOLU,RDSF,0
!*
!***USE ENHANCED ALGORITHM***
FLDATA,ALGR,SEGR,SIMPLEN
!*
!***EXECUTION CONTROLS***
!*
```

```
FLDATA4,TIME,STEP,STSIZE
FLDATA4,TIME,ISTEP,0
FLDATA4,TIME,NUMB,STPS
FLDATA4,TIME,TEND,1.0e06
FLDATA4,TIME,GLOB,10
FLDATA4,TIME,VX,0.01
FLDATA4,TIME,VY,0.01
FLDATA4,TIME,VZ,0.01
FLDATA4,TIME,PRES,1e-006
FLDATA4,TIME,TEMP,1e-006
FLDATA4,TIME,ENKE,0.01
FLDATA4,TIME,ENDS,0.01
FLDATA4A,STEP,OVER,0
FLDATA4,TIME,OVER,0
FLDATA4A,STEP,APPE,5
FLDATA4,TIME,APPE,1.0e6
FLDATA4,STEP,SUMF,20
FLDATA4,TIME,SUMF,1.0e6
FLDATA4,TIME,BC,0
FLDATA4,TIME,METH,NEWM
FLDATA4,TIME,DELTA,0.5
!*
!***MATERIAL PROPERTIES***
FLDATA8,NOMI,DENS,1.0e3
FLDATA8,NOMI,VISC,1.0e-3
FLDATA8,NOMI,SFTS,0.072
FLDATA8,NOMI,WSCA,90
!*
!***MODIFIED REFERENCE PROPERTIES***
FLDATA15,PRES,REFE,101325
FLDATA16,BULK,BETA,2.2e+09
!*
!***GRAVITY***
ACEL,0,9.81,0
!*
!***BOUNDARY CONDITIONS***
!*
SELTOL,0.0000001
!*
!***OUTER BOUNDARIES***
NSEL,S,LOC,X,0
D,ALL,VX,0
NSEL,S,LOC,X,RADIUS
D,ALL,VX,0
ALLS
!*
!***OPENING***
LSEL,S,LOC,Y,HEIGHT,,,0
DL,ALL,1,PRES,0,0
!*
!***DRIVING SURFACE***
LSEL,S,LOC,Y,0,,,0
DL,ALL,1,ENKE,-1,0
!*
!-->
*SET,_FNCNAME,'FLO'
*SET,_FNCCSYS,0
! /INPUT,flo.func,,,1
*DIM,%_FNCNAME%,TABLE,6,10,1,,,,%_FNCCSYS%
!*
! Begin of equation: AMPLI*sin(2*{PI}*FRQC*{TIME})
*SET,%_FNCNAME%(0,0,1), 0.0, -999
*SET,%_FNCNAME%(2,0,1), 0.0
*SET,%_FNCNAME%(3,0,1), 0.0
```

```
*SET,%_FNCNAME%(4,0,1), 0.0
*SET,%_FNCNAME%(5,0,1), 0.0
*SET,%_FNCNAME%(6,0,1), 0.0
*SET,%_FNCNAME%(0,1,1), 1.0, -1, 0, 2, 0, 0, 0
*SET,%_FNCNAME%(0,2,1), 0.0, -2, 0, 3.14159265358979310, 0, 0, -1
*SET,%_FNCNAME%(0,3,1),   0, -3, 0, 1, -1, 3, -2
*SET,%_FNCNAME%(0,4,1), 0.0, -1, 0, FRQC, 0, 0, -3
*SET,%_FNCNAME%(0,5,1), 0.0, -2, 0, 1, -3, 3, -1
*SET,%_FNCNAME%(0,6,1), 0.0, -1, 0, 1, -2, 3, 1
*SET,%_FNCNAME%(0,7,1), 0.0, -1, 9, 1, -1, 0, 0
*SET,%_FNCNAME%(0,8,1), 0.0, -2, 0, AMPLI, 0, 0, -1
*SET,%_FNCNAME%(0,9,1), 0.0, -3, 0, 1, -2, 3, -1
*SET,%_FNCNAME%(0,10,1), 0.0, 99, 0, 1, -3, 0, 0
! End of equation: AMPLI*sin(2*{PI}*FRQC*{TIME})
!-->
!*
DL,ALL,1,UY,%FLO%,0
!*
!***INITIAL LIQUID LOCATION***
NSEL,S,LOC,Y,0,DEPTH
ESLN,S,1
ICE,ALL,VFRC,1
ALLS
FINISH
!*
!***INITIALIZE ALL***
/SOL
FLOCHECK,1
!*
!***DISPLAY LIQUID LOCATION***
/POST1
SET,LAST
PLVFRC,0
FINISH
SAVE
!*
!***SOLVE***
/SOL
SOLVE
FINISH
SAVE
!*
!***ANIMATE Y VELOCITY***
/POST1
!*
PLNS,V,Y
ANDATA,0.05,,0,0,0,1,0,1
FINISH
SAVE
```

Appendix B

MATLAB Code

178.6 kHz Case (sample)

```
clear all
close all
clc

% Material Properties
mu=0.001;                                  % Pa*s
rho=1000;                                  % kg/m^3
sig=0.072;                                 % J/m^2

% Design Parameters
f=178571;                                  % Hz (actuator frequency)

% Atomization Inception

%ac=2*(mu/rho)*(rho/(pi*sig*f))^(1/3)

% Wave Properties (Kelvin)
lamK=((8*pi*sig)/(rho*(f^2)))^(1/3)        % surface wavelength

% Droplet Properties (Lang)
D32K=lamK*0.34                             % droplet mean diameter (m)
%D=D32K*1e6;                               % microns
%d=0:1:60;                                 % array, droplet diameter
%fd=128/(3*D^4)*(d.^3).*exp(-4*d/D)        % probability density
%plot(d,fd)
%xlabel('Droplet diameter (um)')
%ylabel('Probability')
rK=D32K/2;                                 % radius
VK=4/3*pi*rK^3;                            % droplet volume
SK=4*pi*rK^2;                              % droplet surface area

% Wave Properties (ANSYS)
U=8;                                       % maximum wave tip velocity

% Energy
Evib=0.5*rho*VK*(U^2)                      % kinetic energy per droplet
Evis=4*VK*mu*f                             % viscous resistance energy
Est=sig*SK                                 % surface tension resistance
energy
Eform=Est+Evis;
ratio=Evib/Eform
```

REFERENCES

[1] Waldrep, J. C., and R. Dhand. "Advanced Nebulizer Designs Employing Vibrating Mesh/Aperture Plate Technologies for Aerosol Generation." *Current Drug Delivery* 5.2 (2008): 114-119.

[2] Su, Guoguang, P. Worth Longest, and Ramana M. Pidaparti. "A Novel Micropump Droplet Generator for Aerosol Drug Delivery: Design Simulations." *Biomicrofluidics* 4.4 (2010): 044108.

[3] Huang, Y.L., and S.H. Chang. "Micro-Droplets Atomizer Using PZT Ring Actuator." *Journal of Mechanics* 26.3 (2010): 423-429.

[4] Shen, S.C. "A New Cymbal-shaped High Power Microactuator for Nebulizer Application." *Microelectronic Engineering* (2009).

[5] Maehara, Naoyoshi, Sadayuki Ueha, and Eiji Mori. "Influence of the Vibrating System of a Multipinhole-plate Ultrasonic Nebulizer on Its Performance." *Review of Scientific Instruments* 57.11 (1986): 2870.

[6] Dhand, Rajiv. "New Frontiers in Aerosol Delivery During Mechanical Ventilation." *Respiratory Care* 49.6 (2004): 666-677.

[7] Elhissi, A., M. Faizi, W. Naji, H. Gill, and K. Taylor. "Physical Stability and Aerosol Properties of Liposomes Delivered Using an Air-jet Nebulizer and a Novel Micropump Device with Large Mesh Apertures." *International Journal of Pharmaceutics* 334.1-2 (2007): 62-70.

[8] Eslamian, Morteza, and Nasser Ashgriz. "Effect of Atomization Method on the Morphology of Spray-Generated Particles." *Journal of Engineering Materials and Technology* 129.1 (2007): 130.

[9] Watts, Alan B., Jason T. McConville, and Robert O. Williams. "Current Therapies and Technological Advances in Aqueous Aerosol Drug Delivery." *Drug Development and Industrial Pharmacy* 34.9 (2008): 913-922.

[10] Arulmuthu, Eugene R., David J. Williams, Helen Baldascini, Henk K. Versteeg, and Mike Hoare. "Studies on Aerosol Delivery of Plasmid DNA Using a Mesh Nebulizer." *Biotechnology and Bioengineering* 98.5 (2007): 939-955.

[11] Ghazanfari, Thu, Abdelbary M.A. Elhissi, Zhiyi Ding, and Kevin M.G. Taylor. "The Influence of Fluid Physicochemical Properties on Vibrating-mesh Nebulization." *International Journal of Pharmaceutics* 339.1-2 (2007): 103-111.

[12] Lang, Robert J. "Ultrasonic Atomization of Liquids." *The Journal of the Acoustical Society of America* 34.1 (1962): 6.

[13] Benjamin, T. B., and F. Ursell. "The Stability of the Plane Free
Surface of a Liquid in Vertical Periodic Motion." *Proceedings of
the Royal Society A: Mathematical, Physical and Engineering
Sciences* 225.1163 (1954): 505-515.

[14] Lamb, Horace. *Hydrodynamics*. 6th ed. New York: Dover
Publications, 1945. 455-60.

[15] Peskin, Richard L., and Roland J. Raco. "Ultrasonic Atomization of
Liquids." *The Journal of the Acoustical Society of America* 35.9
(1963): 1378-1381.

[16] Al-Suleimani, A. J. Yule, Y. "On Droplet Formation from Capillary
Waves on a Vibrating Surface." *Proceedings: Mathematical,
Physical and Engineering Sciences* 456.1997 (2000): 1069-1085.

[17] Sindayihebura, D., and L. Bolle. "Theoretical and Experimental
Study of the Behavior of Liquid Film Free Surfaces Driven by
Transverse Ultrasonic Vibrations." *Computational Modeling of
Free and Moving Boundary Problems* 3 (1995): 67-74.

[18] Dobre, M., and L. Bolle. "Visualization and Analysis of Liquid Film
Surface Patterns Formed on Ultrasonic Atomisers." *sites-
final.uclouvain.be*. Department of Mechanical Engineering -
Université Catholique De Louvain, 5 July 1999. Web.

[19] Sindayihebura, Daniel, Leon Bolle, Alain Cornet, and Luc Joannes.
"Theoretical and Experimental Study of Transducers Aimed at

Low-frequency Ultrasonic Atomization of Liquids." *The Journal of the Acoustical Society of America* 103.3 (1998): 1442-1448.

[20] Al-Suleimani, Y., A. J. Yule, and A. P. Collins. "How Orderly is Ultrasonic Atomization?" *yjcorp.co.kr*. Department of Mechanical Engineering, UMIST, 5 July 1999. Web.

[21] Willard, G. W. "Ultrasonically Induced Cavitation in Water: A Step-by-Step Process." *The Journal of the Acoustical Society of America* 25.4 (1953): 669.

[22] Antonevich, J.N. "Ultrasonic Atomization of Liquids." *Transactions of the IRE Professional Group on Ultrasonic Engineering* 6.1 (1959): 6-15.

[23] Kirpalani, D.M., and F. Toll. "Revealing the Physicochemical Mechanism for Ultrasonic Separation of Alcohol–Water Mixtures." *Journal of Chemical Physics* 117.8 (2002): 3874.

[24] Eknadiosyants, O. "Role of Cavitation in the Process of Liquid Atomization in an Ultrasonic Fountain." Soviet Physics-Acoustics, Vol 14, No 1 (July-September 1968) Pp 80–84." *Ultrasonics* 7.1 (1969): 78.

[25] Topp, Michael N. "Ultrasonic Atomization - a Photographic Study of the Mechanism of Disintegration." *Journal of Aerosol Science* 4.1 (1973): 17-25.

[26] Boguslavskii, Y.Y., and O.K. Eknadiosyants. "Physical Mechanism of Acoustic Atomization of a Liquid." Boguslavskii, Y.Y., Eknadiosyants, O.K., Soviet Physics-Acoustics, Vol 15, No 1 (July–September 1969): 14–21.

[27] Alzuaga, S., J. Manceau, and F. Bastien. "Motion of Droplets on Solid Surface Using Acoustic Radiation Pressure." *Journal of Sound and Vibration* 282.1-2 (2005): 151-162.

[28] Palan, Vikrant, and W. Steve Shepard Jr. "Enhanced Water Removal in a Fuel Cell Stack by Droplet Atomization Using Structural and Acoustic Excitation." *Journal of Power Sources* 159.2 (2006): 1061-1070.

[29] Wang, Wei-Ning, Agus Purwanto, I. Wuled Lenggoro, Kikuo Okuyama, Hankwon Chang, and Hee Dong Jang. "Investigation on the Correlations between Droplet and Particle Size Distribution in Ultrasonic Spray Pyrolysis." *Industrial & Engineering Chemistry Research* 47.5 (2008): 1650-1659.

[30] Avvaru, B., M. Patil, P. Gogate, and A. Pandit. "Ultrasonic Atomization: Effect of Liquid Phase Properties." *Ultrasonics* 44.2 (2006): 146-158.

[31] Sindayihebura, D., M. Dobre, and L. Bolle. "Experimental Study of Thin Liquid Film Ultrasonic Atomization." *sites-final.uclouvain.be*. Department of Mechanical Engineering - Université Catholique De Louvain. Web.

[32] Kumar, Satish. "Parametrically Driven Surface Waves in Viscoelastic Liquids." *Physics of Fluids* 11.8 (1999).

[33] Rajan, R., and A.B. Pandit. "Correlations to Predict Droplet Size in Ultrasonic Atomization." *Ultrasonics* 39.4 (2001): 235-255.

[34] Hedrih, K., V. Babovic, and D. Sarkovic. "An Auxiliary Size Distribution Model for the Ultrasonically Produced Water Droplets." *Experimental Thermal and Fluid Science* 30.6 (2006): 559-564.

[35] Barreras, F., H. Amaveda, and A. Lozano. "Transient High-frequency Ultrasonic Water Atomization." *Experiments in Fluids* 33.3 (2002): 405-413.

[36] Dumouchel, Christophe, Daniel Sindayihebura, and Leon Bolle. "Application of the Maximum Entropy Formalism on Sprays Produced by Ultrasonic Atomizers." *Particle and Particle Systems Characterization* 20.2 (2003): 150-161.